Bionic Design and Analysis of a Novel Quadruped Robot with a Multistage Buffer System

Yi Zheng, Kun Xu, Yaobin Tian, Huichao Deng[*] and Xilun Ding

Abstract

Large quadruped mammals, such as ruminants, have outstanding motion ability, including running and bounding. These advanced motion abilities are related to the buffer effect of their complicated musculoskeletal systems. However, the buffer effect of most bio-robots is not satisfactory owing to the simple design of their buffer systems. In this paper, a physiological analysis of the ruminant musculoskeletal system is presented to explain the intrinsic buffer mechanism of motion. Based on the physical buffer parts of the ruminant limbs, the corresponding bionic mappings were determined. These mappings were used to guide the mechanism design of the robot multistage buffer system. The multistage buffer system includes two main buffer mechanisms: the first stage and the second stage. The buffer mechanism analysis of the first stage and multiple stages is discussed in theory to compare the effects between the normal single buffer system and the novel multistage buffer system. Then, the detailed mechanical structure of the limbs was designed based on the limb mechanism design. To further verify the superior efficacy of the multistage buffer system, the corresponding walking simulation experiments were conducted after the virtual prototype of a quadruped robot with a novel limb was built completely. Both theoretical analysis and simulation experiments prove that the bionic robot design with the novel multistage buffer system achieves better motion performance than the traditional robot buffer design and can be regarded as the design template of the robot limb.

Keywords: Ruminant musculoskeletal system, Bioinspired multistage buffer system, Mechanism design, Robotics, Quadruped robot

1 Introduction

According to the motion mode, a general terrain mobile robot can be classified into three types: wheeled, tracked, and legged. Compared with the previous two types, the legged robot possesses better terrain adaptability and can realize various functions such as continuous walking under rough terrain, obstacle crossing, and self-recovery from an overturned state. Moreover, under the same constraint conditions, such as motion stability and structure size, a quadruped robot can achieve a higher speed compared with other types of legged robots. Given

comprehensive factors such as manufacturing cost and difficulty of control, the high efficiency ratio is also a primary reason why quadruped robots have become one of the most popular topics in robot research.

When the quadruped robot realizes the basic walking function, the change in the environment will directly affect the robot motion performance, such as the speed threshold and walking stability. The most effective method for mitigating the negative influence of the environment is the optimal design of the robot legs. Therefore, scholars from various countries have conducted extensive research on this topic. As early as 1990, Alexander [1] conducted research on three uses of springs in legged locomotion. These three uses are the pogo stick, return springs, and foot pads. However,

*Correspondence: denghuichao@buaa.edu.cn
School of Mechanical Engineering and Automation, Beihang University, Beijing 100191, China

Zheng *et al. Chinese Journal of Mechanical Engineering*   (2022) 35:32

Page 2 of 21

in the early design of traditional robot mechanical legs, most researchers considered only one use of the spring. For example, the foot was generally designed in planar, curved, or spherical form and assisted by springs or other damping devices to reduce vibration. For instance, the BigDog robot developed by Boston Dynamics is a representative prototype [2–7]; its feet are cylindrical and made up of rubber material. Damper springs, which are installed in the metacarpal, are used for vibration reduction and energy storage. Apart from adding springs to the robot legs as in BigDog, an additional prototype StarlETH [8–10] was developed by ETH Zürich. This robot can gain power through the compliant mechanism of joints, which is inspired by natural creatures. Owing to the rise of bionics, various bionic leg structure designs have been applied to robot leg design to improve the performance of robot legs. For example, researchers at the MIT Biomimetic Robotics Laboratory developed a type of quadruped bio-robot called Cheetah [11–14]. The Cheetah robot applies a tendon mechanism formed by Kevlar to connect the foot and knee. To ensure the stiffness and reduce the weight, the shell of the Cheetah leg linkage was made of acrylonitrile butadiene styrene with high stiffness, and the filler was polyester foam. The design of the Cheetah leg follows the animal leg template, which includes a tendon and bone system (a tendon–bone co-location design). The tendon mechanism was embedded in the leg and bypassed the ankle joint. The bones of the leg and foot work under pressure, and the tendon is in tension. This leg structure helps the bones avoid suffering a large bending moment and increases the strength-to-weight ratio of bones. Cheetah-cub [15–19] is a motor-driven quadruped robot developed by EPFL. The leg design of the robot included three springs. One spring was installed at the foot end and played the role of foot pads. Two springs with different stiffnesses were installed in the shank and worked at different velocities. The maximum velocity of Cheetah-cub was 1.4 m/s with a trotting gait.

Similar to the robots mentioned above, in previous research studies on robot leg spring design, researchers focused on the foot end, shank, or metacarpal part of the robot leg and added a damping device to these parts simply and separately. These methods are partly effective, but they ignore the fact that every part of a quadruped limb (e.g., the muscle, cartilago articularis, tendon, and ligament) will participate in the buffer during motion. The use of return springs has not been sufficiently studied. As claimed in Ref. [1], running animals use springs for all three functions, similar to robots. Therefore, the robot spring design with a buffer effect was not satisfactory.

The remainder of this paper is organized as follows: The model is based on the physiological structure of a quadruped ruminant, and the biological buffer structure of a ruminant limb is analyzed anatomically in Section 2.1. Section 2.2 introduces the mapping models. In Section 2.3, the mapping models are applied to the robot leg design, and a novel single-leg structure design with a multistage buffer system is presented. Moreover, a working mechanism analysis of buffer systems is presented in this section. Section 3 validates and discusses the buffer effect based on the theory presented in Section 2 through a simulation experiment. Finally, Section 4 concludes the paper.

2 Materials and Methods
2.1 Analysis of Animal Anatomy
Compared with other large quadruped mammals, the body of a typical ruminant (e.g., a mountain goat [20]) is relatively smaller. Its skull is short and wide. The shape of the skull is similar to that of a pyramid; the limb bones are strong and forceful. In particular, ruminants have been proven to have a low center of mass (COM) and a fairly thin body when viewed anteriorly [21]. These structural features lead to the consequence that the moving gaits are agile and quick. Moreover, the gait type is rich (walk, trot, pace, gallop, canter and bound), and the climbing ability of an artiodactyl foot is remarkable. Consequently, a ruminant can walk quickly and freely in different environments, such as on flat ground, slopes, steep walls, etc. The ability of ruminant animals to move is outstanding.

2.1.1 Skeletal Structure of Ruminant Forelimbs
The skeletal system of mammals includes bone and bone unions. Bone supports the entire body and is the basis for realizing body movement. Bone union is a hinge of the body movement. During the motion process, the skeletal system makes it possible for an animal to perform various functions such as self-weight support, load-bearing, and flexible movement in different environments. In large quadruped mammals, such as ruminants, different limbs perform different functions. The forelimbs function mainly as buffers, enabling slowing down and bearing loads. Hindlimbs provide power and speed-up functions [22]. Therefore, the force applied to the forelimbs is generally greater during the motion. Accordingly, the forelimbs of ruminants were selected as the research object in this paper.

From the near-earth side to the near-body side, the main bones of the forelimb are the pedal bone, coronary bone, pastern bone, ossa metacarpalia, radius, ulna, humerus, and scapula [23]. As shown in Figure 1, the main joints of the forelimb are articulationes interphalangeae distales manus, articulationes interphalangeae proximales manus, articulationes metacarpophalangeae, articulatio carpi (wrist joint), articulatio
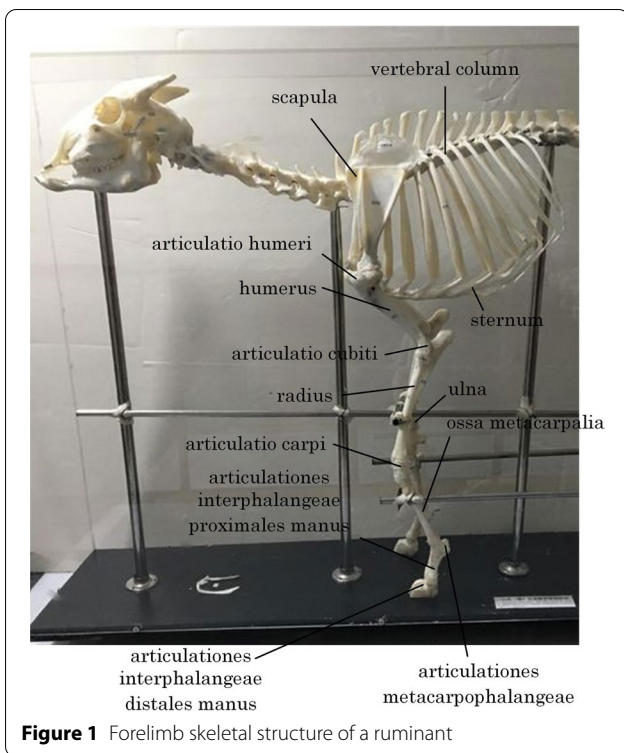
Zheng *et al. Chinese Journal of Mechanical Engineering*   (2022) 35:32

Page 3 of 21

Figure 1 Forelimb skeletal structure of a ruminant

cubiti (elbow joint), and articulatio humeri (shoulder joint). The forelimb skeletal system of a ruminant is composed of bones and joints.

According to the skeletal system diagram, in the most traditional leg design of a legged robot, the connecting links mainly refer to the humerus (thigh), radius (shank), and ossa metacarpalia. The lower parts of the ossa metacarpalia were simplified into a single segment. The scapula was generally fixed with the robot. Joint design mainly refers to the shoulder, elbow, and

wrist joints, which are the three joints near the ground that are generally ignored.

2.1.2 Muscle System of Ruminant Forelimbs

During animal motion, a transfer of force between the animal limbs and the ground exists. This force can be regarded as the impact of the ground against the animal body during motion. The motion impact, which acts on the animal, is related not only to the physiological structure but also to the motion mode, motion environment of the animal, etc. The muscle system and ligaments of an animal can function as a buffer system. Each part of the equivalent buffer system can protect the organs and tissues of the body from the damage caused by motion impact by working coordinately. Through this means, the motion impact on the animal can be buffered.

In traditional robot leg design, a three-section leg is the most popular design template. In general, only one buffer mechanism is placed in the metacarpal, thigh, or shank simply without considering that the scapula is not rigidly fixed on the body. Only one buffer mechanism takes effect, and the buffer effect of a traditional robot leg is not satisfactory. Therefore, an anatomical analysis of the shoulder muscle system for optimizing the buffer mechanism design will be introduced in the following.

During the process in which the foot and the ground come into contact (henceforth referred to as foot–ground contact), the position of the scapula ascends, while the animal body descends relatively. Moreover, during this process, the pectoralis and ventral muscles will undergo a stretching motion. Meanwhile, the trapezius, deltoid, and latissimus dorsi undergo compressed motion. The main muscle groups are shown in Figures 2 and 3, respectively. Muscle movements apply force to the leg structure and reduce motion impact.

According to the analysis of the ruminant forelimb shoulder muscle system, the coordinating motion of
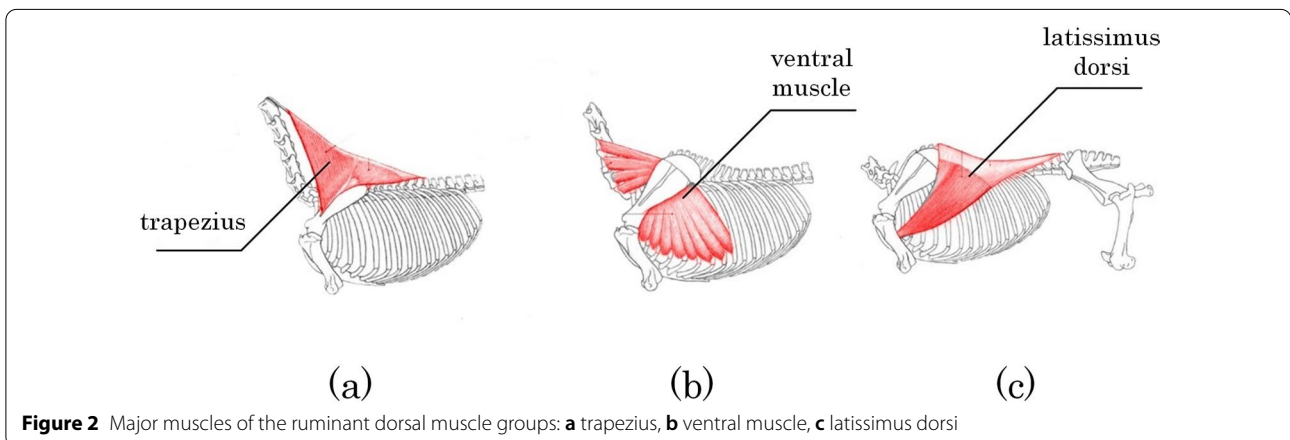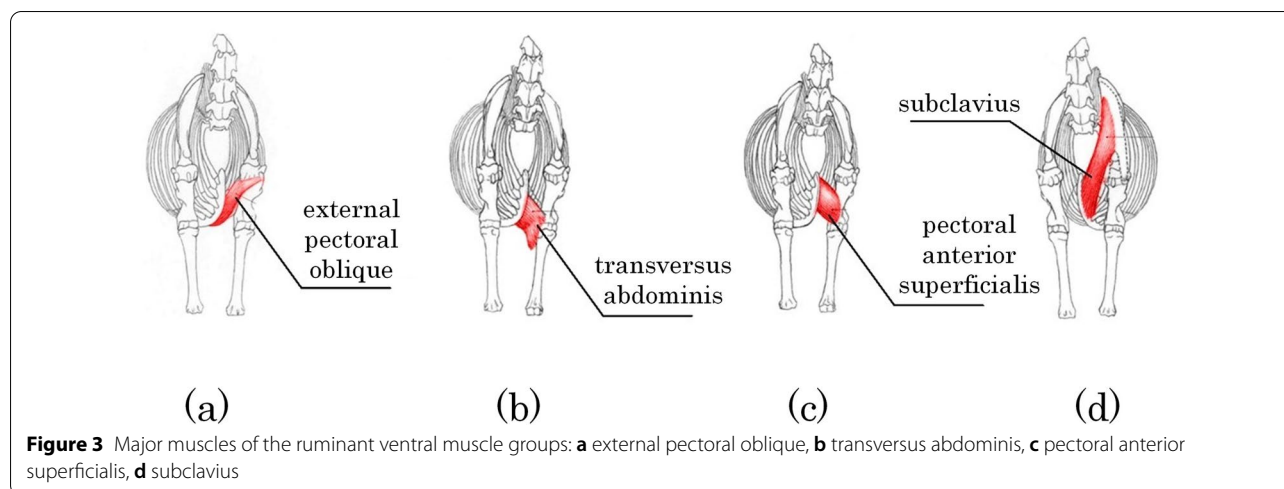

Figure 2 Major muscles of the ruminant dorsal muscle groups: **a** trapezius, **b** ventral muscle, **c** latissimus dorsi

Zheng *et al. Chinese Journal of Mechanical Engineering*   (2022) 35:32

Page 4 of 21

Figure 3 Major muscles of the ruminant ventral muscle groups: **a** external pectoral oblique, **b** transversus abdominis, **c** pectoral anterior superficialis, **d** subclavius

every part of the shoulder can not only support and maintain the internal structural stability of the body but also coordinate the movement of the forelimb and mitigate the motion impact that acts on the body. Therefore, a shoulder buffer system is formed.

Next, anatomical analysis of each part of the limb should be considered. Among the endmost muscles of the leg, some parts almost lose the muscle fiber and become the so-called tendon, which is similar to a spring [24]. During foot–ground contact, these tendons can store elastic potential energy similar to springs when the muscles are stretched. When the muscles contract, the tendons release this energy and provide power for movement. Therefore, this mechanism enables the ruminant to walk with a light-footed, energy-conserving gait without load and can absorb the motion impact from its own load and an external load.

The hoof structure of a ruminant foot end can greatly reduce the motion impact from the ground, and the tendon that is attached to the foot end can buffer the motion impact, lowering high-frequency vibration [25, 26]. The tendon is a dense connective tissue that connects the belly muscle and bone. Similar to the tendon, the ligament is also a type of dense connective tissue, but a ligament mainly connects the bone, bone, or joint and joint. During foot–ground contact, joint rotation stretches and deforms the ligaments of the foot and produces elastic force and elastic potential energy because of the reaction force from the ground. When the reaction force of the ground diminishes, ligaments contract and release energy. This event provides power for the subsequent motion. Moreover, the intracapsular and extracapsular ligaments of the joints in the ruminant foot will limit the joint lateral rotation and ensure that the joints can rotate in the proper range. The joints can be passively stabilized.

The distributions of the main tendons and ligaments in the ruminant forelimb are shown in Figure 4.

The tendons and ligaments at the end of the limb form a tendon–ligament system, which can store energy as well as buffer and reduce vibration in the process of animal motion. Long tendons connected to each end of the muscle are attached to the bone. The skeletal system can work normally with tendon traction. Meanwhile, the joint rotates passively in a small range when the limb is impacted by motion. This is caused by the tendons and ligaments. Therefore, a tendon–ligament system has a significant effect on buffering the motion impact.

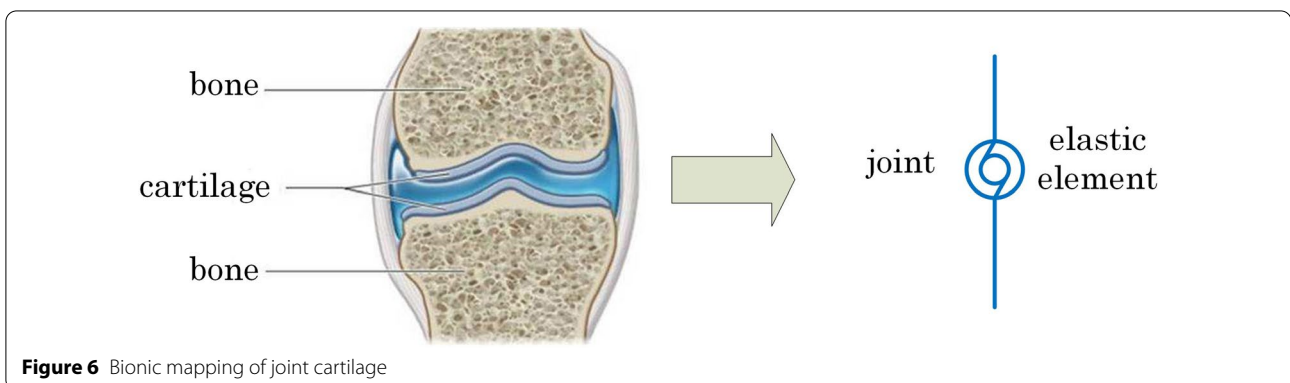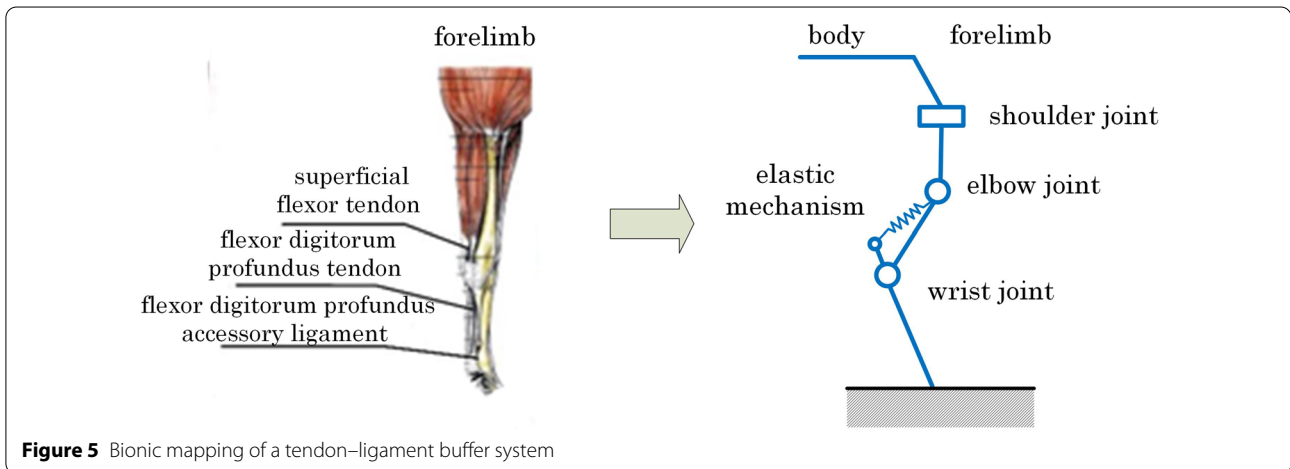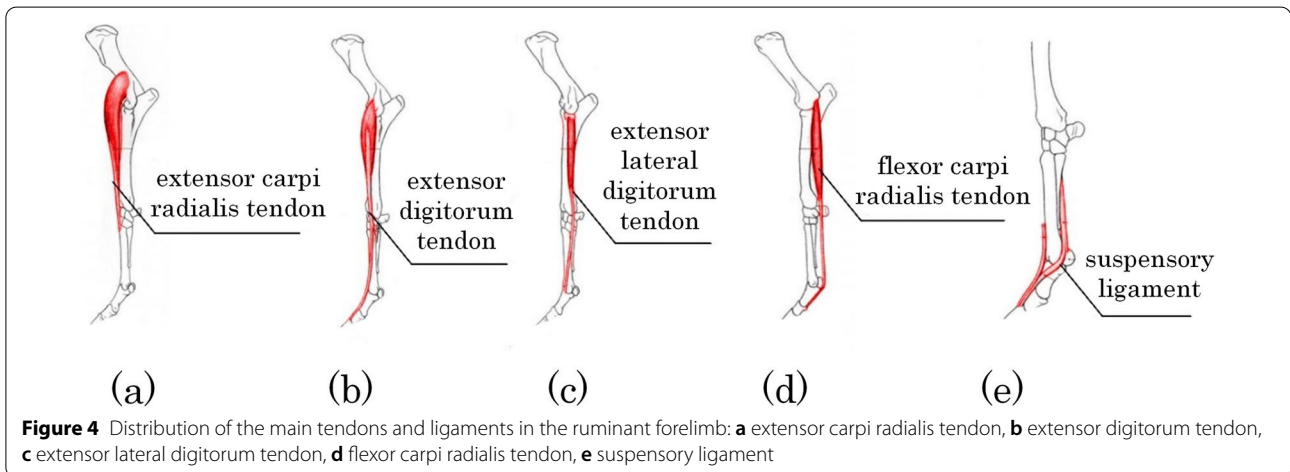## 2.2 Bionic Mapping Models of the Buffer System

In this section, according to the physiological analysis of an animal musculoskeletal system, the motion buffer mechanism is determined. The corresponding bionic mappings are presented based on this intrinsic buffer mechanism. Therefore, these mappings can provide templates for the buffer mechanism design of a legged robot.

In general, during foot–ground contact, the tendon–ligament system buffers the motion impact first. This is equivalent to adding an elastic mechanism to the animal limb, which can enable energy storage as well as buffer and reduce vibration. Therefore, according to the buffer mechanism of the tendon–ligament system, the corresponding bionic mapping model was established, as shown in Figure 5. In the forelimb, an elastic mechanism is added between the wrist and elbow joints. The parts below the wrist joint can be simplified as rigid linkages. This elastic mechanism is stretched and stores energy when the limb touches the ground. When the limb starts to leave the ground, this elastic mechanism contracts and releases energy. Motion impacts can also affect every joint of the limb. In particular, owing to the elasticity of

cartilage, the cartilage of the joint plays a major role in impact buffering. The physiological structure of cartilage is shown in Figure 6 [27].

After the preliminary buffer effects of the tendon–ligament system and cartilage, the motion impact is transmitted to the parts that connect the limbs and the body via bones, muscles, and joints. These parts are the shoulder and the hip. According to the analysis of the shoulder (hip) buffer system, which is composed of a shoulder (hip) muscle system, this buffer system is

(a)   (b)   (c)   (d)   (e)

Figure 4 Distribution of the main tendons and ligaments in the ruminant forelimb: **a** extensor carpi radialis tendon, **b** extensor digitorum tendon, **c** extensor lateral digitorum tendon, **d** flexor carpi radialis tendon, **e** suspensory ligament

Figure 5 Bionic mapping of a tendon–ligament buffer system

Figure 6 Bionic mapping of joint cartilage

Zheng *et al. Chinese Journal of Mechanical Engineering* (2022) 35:32

Page 6 of 21

equivalent to building a bridge between the limbs and the body to realize the smooth movement of limbs and buffer the motion impact. As shown in Figure 7, a bionic mapping model of the shoulder (hip) muscle system was established. In this model, an elastic mechanism equal to the shoulder (hip) was added between the body and limbs. The impact of the buffer process of the shoulder (hip) buffer system is similar to that of the tendon–ligament buffer system. Moreover, except for the motion impact buffer function, the shoulder (hip) buffer system can ensure the stability of the body and smooth transition of the COM. High energy efficiency and high stability can be achieved by combining the tendon–ligament buffer system and the shoulder (hip) muscle system.

2.3 Bionic Limb Design with a Buffer Function

In general, the joints and leg structures of a legged robot are purely rigid. In this case, the merit is that accurate position control of the foot end can be realized. However, the loading capacity of a legged robot is mainly reflected in its movement. When a robot is working in a rough and complex environment, the rigid leg and joint may be damaged and incapacitated because of the acute motion impact. The robot's own weight and external loading will cause an impact during the motion process, and this impact may damage the driving motors and mechanical structure of the robot. According to the analysis of animal anatomy, the motion impact can be buffered by animal muscles, tendons, ligaments, etc. Consequently, energy storage and impact buffering can be achieved. Based on bionics, a flexible mechanism should be added to the robot leg to buffer the motion impact and improve the dynamic motion ability of a legged robot.

2.3.1 Mechanism Design of the Multistage Buffer System

The main types of quadruped robot legs are insectile and mammalian [28, 29]. Compared with the former type, the four legs of a mammalian quadrupedal robot are under the body. There are three main driving joints: the shoulder, elbow, and wrist joints (for forelimbs). The shoulder joint is responsible for the lateral swing of the limbs, while the elbow and wrist joints are responsible for the front kick and retral swing of the limbs cooperatively.

First, the buffer function of the joint cartilage should be considered because this buffer mechanism is relatively simple. For forelimbs, a torsional spring–damper mechanism can be added to the wrist joint, as shown in Figure 8a. However, according to the anatomy analysis in the previous section, the buffer effect of a single cartilage is not satisfactory, and the cartilage must be combined with the tendon–ligament system to buffer the motion impact synchronously. Therefore, based on the bionic mapping of the tendon–ligament buffer system, a spring–damping system should be added to the lower part of the limb. The spring–damping system can be added between the foot end and wrist joint according to the distribution of the suspensory metacarpal ligament. In this case, a compressed spring was used in the spring–damping system (Figure 8b). In addition, based on the structure of tendons, a tension spring–damping system can be added between the metacarpal and shank, as shown in Figure 8c. A comparison of buffer systems (b) and (c) shows that adding a columnar compressed spring in the metacarpal will make the leg structure complex and increase the metacarpal weight. Therefore, this design is not beneficial for reducing the rotational inertia of the leg. However, the mounting position of the tension spring is relatively higher. In this case, the rotational inertia of the
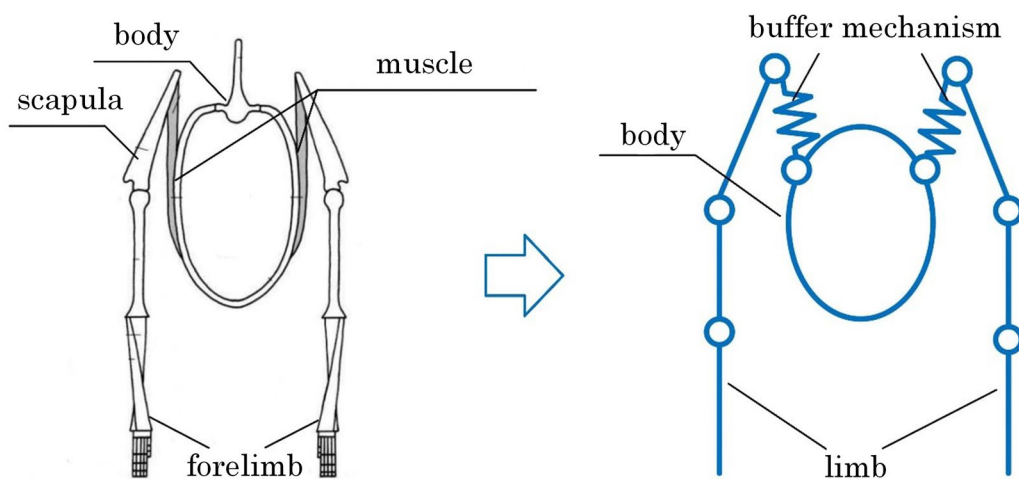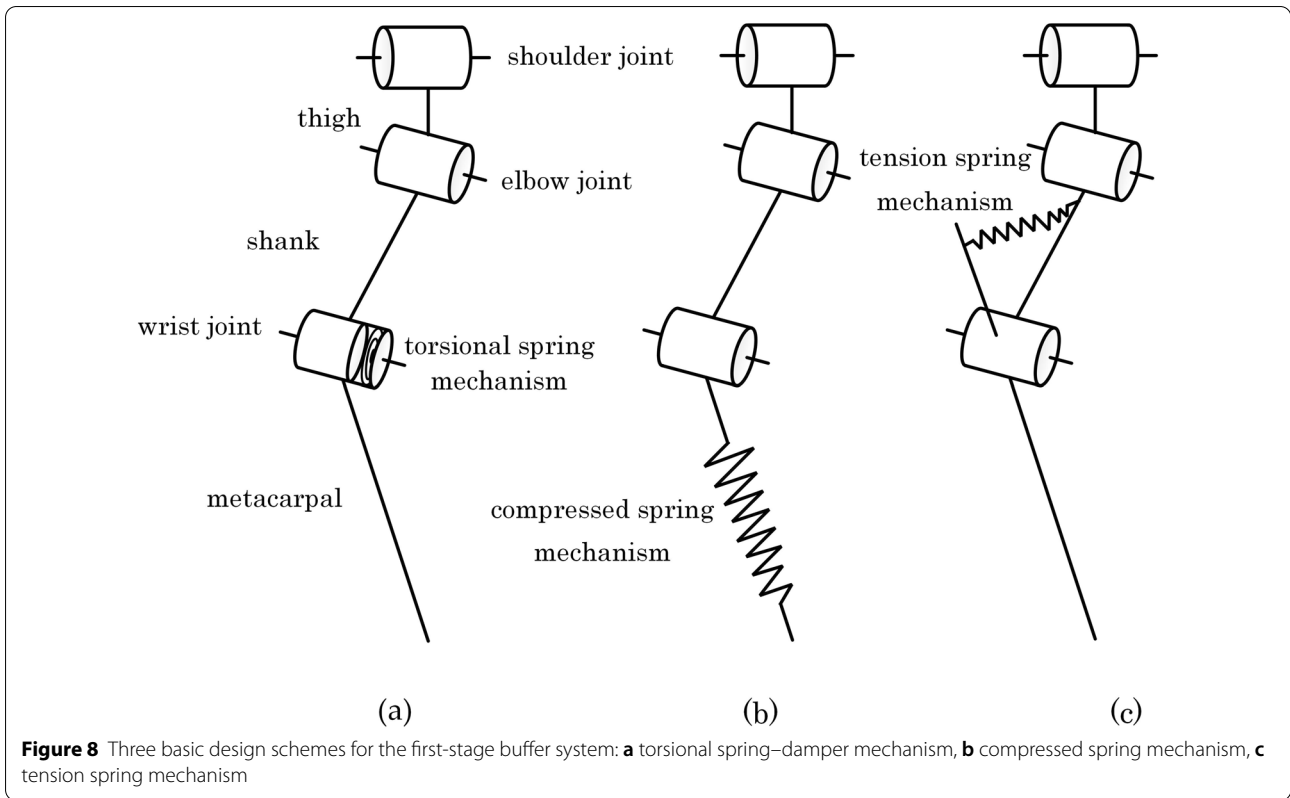

Figure 7 Bionic mapping of the shoulder (hip) buffer system

Zheng *et al. Chinese Journal of Mechanical Engineering*   (2022) 35:32

Page 7 of 21

Figure 8 Three basic design schemes for the first-stage buffer system: **a** torsional spring–damper mechanism, **b** compressed spring mechanism, **c** tension spring mechanism
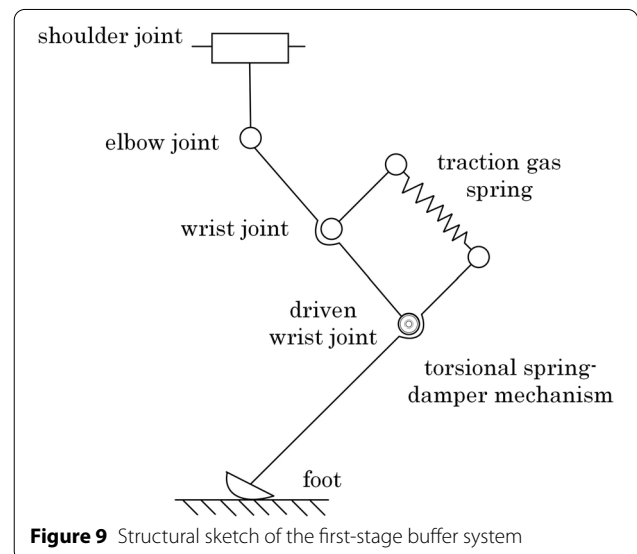
leg did not increase. Moreover, once the structure of the leg is determined, the tension spring mechanism will not affect the workspace of a single leg. Therefore, plan (c) is better than plan (b), and plan (c) should be combined with plan (a) for the design of a first-stage buffer system.

The position of the driving element of the wrist joint can be moved up to further reduce the rotational inertia of the leg. Given this need, a parallelogram mechanism can be applied to complete power transmission. Moreover, a traction gas spring is used as one linkage of the parallelogram mechanism, and this traction gas spring is equal to the buffer element. As a result, the driven wrist joint is generated in the metacarpal, and the metacarpal is driven by the rotation of the driven wrist. Owing to the character of the traction gas spring, this spring will not be compressed by force when the limb is lifted. In this case, the part of the wrist joint is completely rigid, and the control of motion is more accurate. When the limb touches the ground, the traction gas spring is stretched. In this case, the wrist joint part is elastic, and the motion impact is buffered by this mechanism. The energy is stored in the spring and released during the process of leaving the ground. Because the driving element is also mounted in the wrist joint, and the wrist joint should be locked sometime during the motion process, the torsional spring–damper mechanism, which is similar to

cartilage, should be mounted in the driven wrist joint. These two springs constitute the first-stage buffer system, as shown in Figure 9.

Second, the second-stage buffer system model can be established based on the bionic mapping of the shoulder buffer system. As shown in Figure 7, a buffer mechanism

Figure 9 Structural sketch of the first-stage buffer system

Zheng *et al. Chinese Journal of Mechanical Engineering*   (2022) 35:32

Page 8 of 21

that can be equal to the muscle system exists between the limb and body. The shoulder joint connects the buffer mechanism to the thigh. However, in fact, the shoulder joint of a mammal is a typical spheroidal joint, and it should theoretically have a considerable omnidirectional motion, as shown in Figure 10. However, the range of motion of the shoulder joint is limited by muscle restriction. Therefore, the number of degrees of freedom (DOFs) in the design of the shoulder joint can be one to three according to the actual need for robot limb motion. In this paper, adduction and abduction motions were selected as the main DOFs of the shoulder joint. Moreover, the impact buffer of the shoulder requires

Figure 10 Shoulder joint of a ruminant: **a** structural sketch of the equivalent spheroidal joint, **b** physical structure sketch of the shoulder joint

small-range DOFs, which are called flexion and extension DOFs. These DOFs are generated by a newly added joint, which is called a driven shoulder joint. The original second-stage buffer system model is shown in Figure 11.

It is necessary to combine the driven shoulder joint with a buffer system. Here, the parallelogram mechanism is applied to realize flexion and extension DOFs. A type of spring–damping mechanism that can only be unidirectionally compressed owing to the mechanical position limitation is used to limit the range of flexion and extension motion, as shown in Figure 12. When the limb is lifted, the spring does not stretch because of the mechanical position limitation. In this case, the joint is rigid. When the limb touches the ground, the spring is compressed. In this case, the joint part is elastic, and the motion impact is buffered by the spring–damping mechanism. The energy is stored in the spring and released during the process of the foot leaving the ground.

Finally, the first and second buffer systems are combined to form a multistage buffer system, as shown in Figure 13.
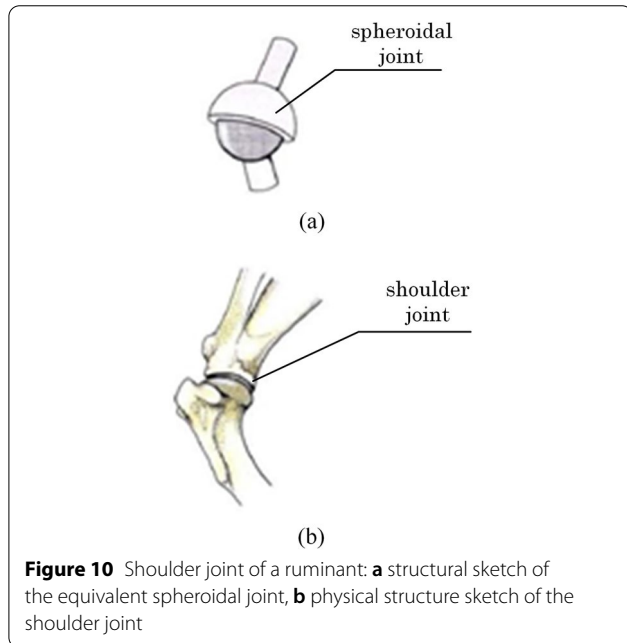
2.3.2 Buffer Mechanism Analysis

The designed single limb structure contains multistage buffer systems, and these buffer systems are connected by a number of rigid driving joints. Consequently, the limb is not a linear vibration system with multiple DOFs. In some cases, every buffer system can buffer the motion impact individually. When the motion impact is buffered only by a first-stage system, the shoulder and wrist joints should be locked, and the elbow joint is used to adjust the pose of the limb. The torsional spring–damper mechanism and traction gas spring work together to buffer the motion impact, and the second-stage buffer system is locked by the mechanical position limitation during this
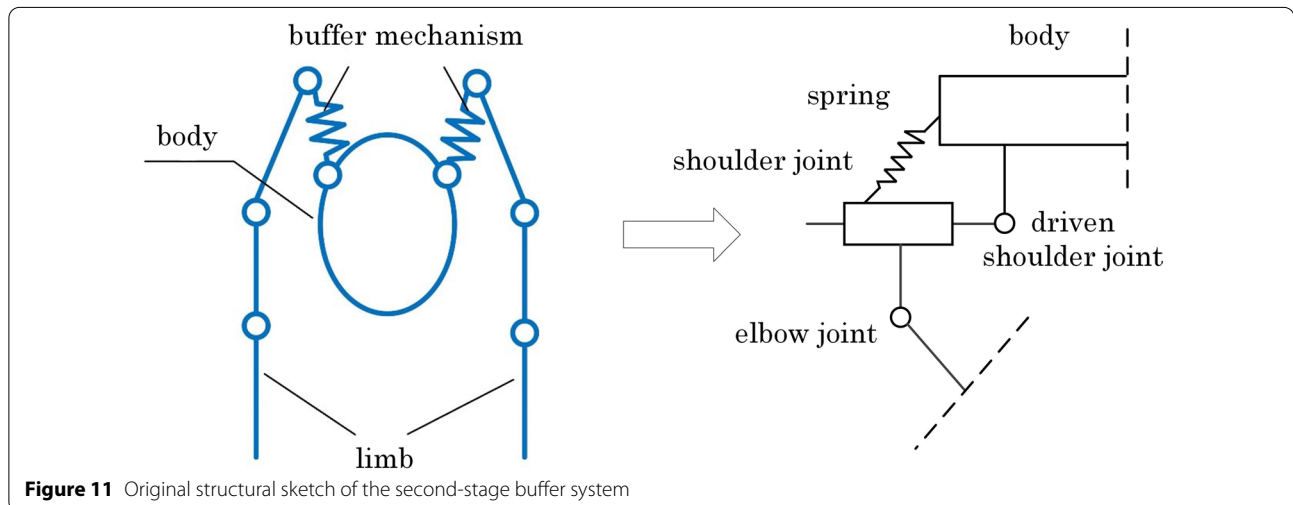

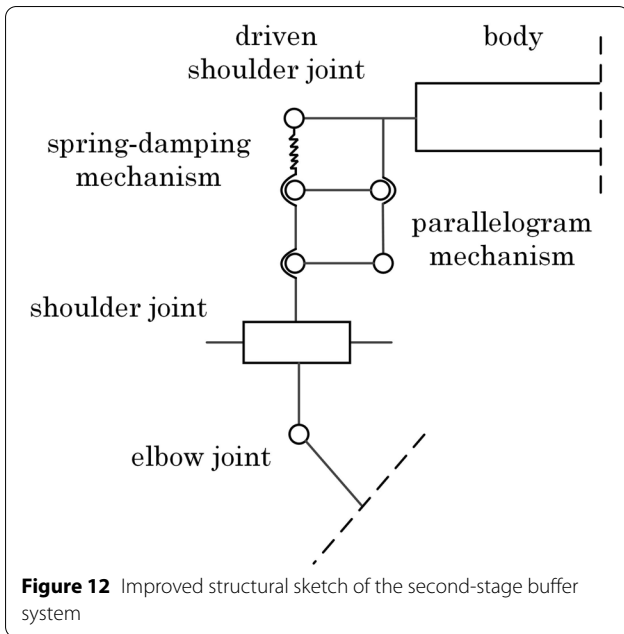**Figure 11** Original structural sketch of the second-stage buffer system

Zheng *et al. Chinese Journal of Mechanical Engineering*　　(2022) 35:32

Page 9 of 21

Figure 12 Improved structural sketch of the second-stage buffer system
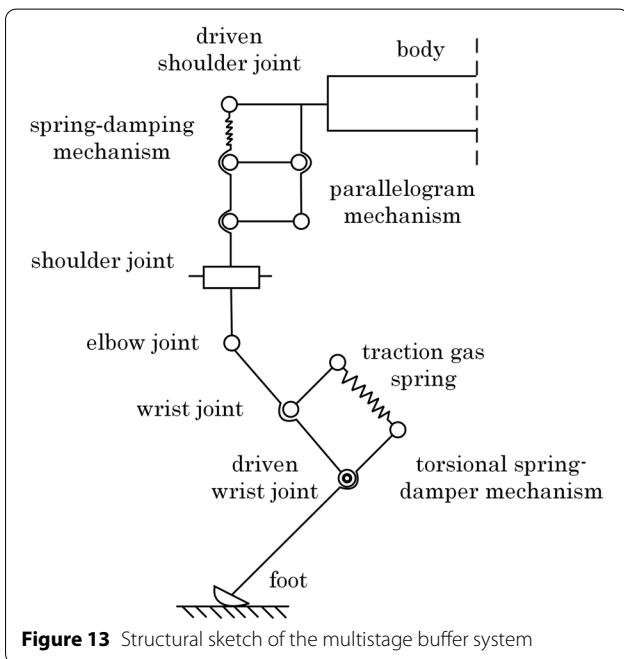

Figure 13 Structural sketch of the multistage buffer system

process. This case is suitable for a small motion impact. When the motion impact is relatively large, in addition to the buffer effect of the first-stage buffer system, the impact is transmitted to the second-stage buffer system, and the second-stage buffer system is deployed. In this paper, based on the buffer mechanism analysis of the first-stage buffer system, an analysis of the whole buffer mechanism is presented.

I. First-Stage Buffer System

For the first-stage buffer system, its buffer mechanisms are a traction gas spring with a damping effect and a torsional spring–damper mechanism. The traction gas spring is in the shortest state when it is not stretched. In fact, when the limb contacts the ground with different loads and speeds, the impact force acting on the limb is also different. Only the impact force reaches the threshold value; it is necessary to use elastic joints to buffer the impact. In this section, the buffer mechanism analysis of the first-stage buffer system is discussed.

When the limb touches the ground, the traction gas spring is in the stretching phase owing to the tension force. We assume that, in this case, the motion impact is not sufficiently large, and the second-stage buffer system is locked as a rigid linkage. Therefore, the equivalent model of the first-stage buffer system can be determined, and the equivalent process is shown in Figure 14.

In Figure 14, m_1 is the equivalent mass of 1/2 of the robot body weight and partial weight of the joints. (We assume that a trotting gait is applied, and we compared with the equivalent mass block and ignored the weight of linkages.) The velocity of m_1 is v_1. α is the angle between the short and long linkages of the parallelogram mechanism, which is connected to the wrist joint. When the foot makes contact with the ground and the collision is elastic, the wrist joint is locked and, during the contact process, α is constant ($\alpha = 90°$).

As shown in Figure 15, state I is the initial state when the foot makes contact with the ground. At this moment, the traction gas spring is still rigid, and the quadrangle $ABCD$ is rectangular. The line connecting the COM of m_1 and the supporting point of the foot is perpendicular to the horizontal plane. After a while, the traction gas spring is stretched by force from the metacarpal, but no slip of the foot end appears. Therefore, BC rotates at point B, and this process is represented as state II.

We define the angle BDC as ∂. According to the geometrical relationship,

$$\partial = \pi - \theta_0 - \arctan\frac{l_2}{l_3} - \varphi, \tag{1}$$

where θ_0 is the constant angle between the thigh and the horizontal plane (where we assume that the robot body stays horizontal and the elbow joint is locked in the contact process); l_2 and l_3 are the short and long linkage lengths of the parallelogram mechanism, respectively; and φ is the angle between the metacarpal and the ground (whose initial value is φ_0).

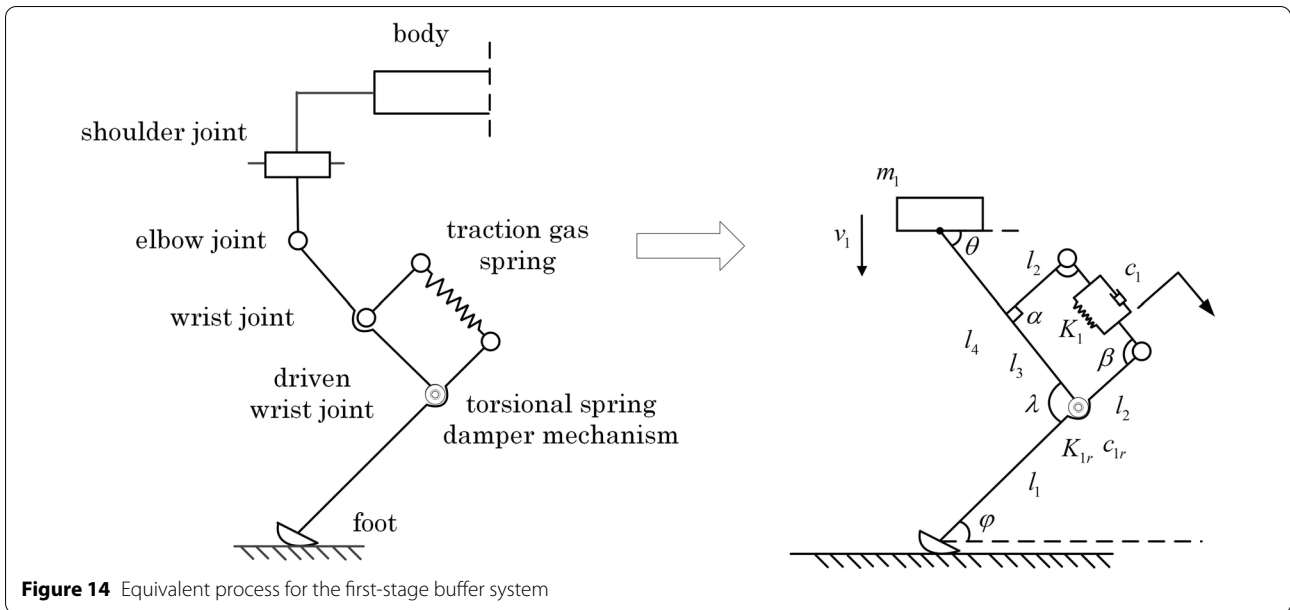According to the cosine law, the length of BC in state II is

Zheng *et al. Chinese Journal of Mechanical Engineering* (2022) 35:32

Page 10 of 21

Figure 14 Equivalent process for the first-stage buffer system

$$l_{BC} = \sqrt{2l_2^2 + l_3^2 - 2l_2\sqrt{l_2^2 + l_3^2}\cos\partial}. \tag{2}$$

The length variation of the traction gas spring, ΔS, is

$$\begin{aligned}\Delta S &= l_{BC} - l_3 \\ &= \sqrt{2l_2^2 + l_3^2 + 2l_2\sqrt{l_2^2 + l_3^2}\cos(\theta_0 + \arctan\frac{l_2}{l_3} + \varphi)} - l_3.\end{aligned} \tag{3}$$

The angle between the metacarpal and the shank is λ; therefore, the angle variation of the torsional spring, $\Delta\lambda$, is

Figure 15 Tension process for the first-stage buffer system

$$\Delta\lambda = \varphi - \varphi_0. \tag{4}$$

It is obvious that both the length variation and angle variation are functions of φ. Generalized coordinates of φ can therefore be established, and the origin was set at the supporting point. The anticlockwise direction was set as positive.

The velocity v_1 can be decomposed into the horizontal component v_{1x} and the vertical component v_{1y}. During the process in which the limb changes from state I to state II, the horizontal displacement of m_1 is

$$s_x = l_1\cos\varphi - l_4\cos\theta_0, \tag{5}$$

where l_1 is the distance from the driven wrist joint to the foot end (the length of the metacarpal) and l_4 is the distance from the elbow joint to the driven wrist joint.

The vertical displacement of m_1 is

$$s_y = l_1(\sin\varphi_0 - \sin\varphi). \tag{6}$$

Therefore, v_{1x} and v_{1y} can be written as

$$v_{1x} = s'_x = l_1\dot{\varphi}\sin\varphi, \tag{7}$$

$$v_{1y} = s'_y = l_1\dot{\varphi}\cos\varphi. \tag{8}$$

The kinetic energy of the first-stage buffer system is

$$V = \frac{1}{2}m_1(s'^2_x + s'^2_y) = \frac{1}{2}m_1 l_1^2\dot{\varphi}^2. \tag{9}$$

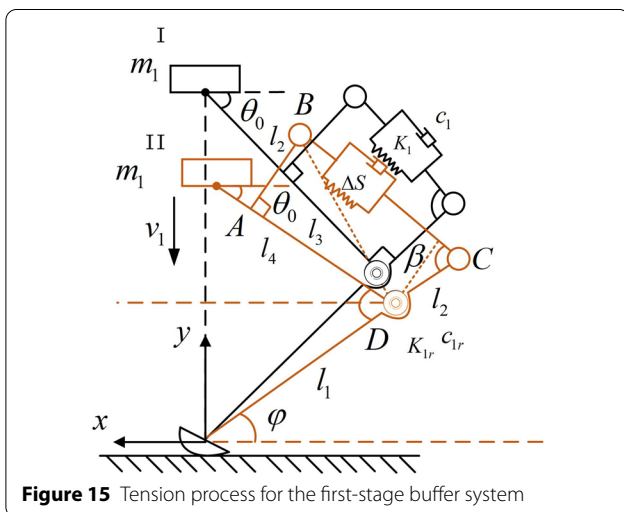The potential energy of the first-stage buffer system is composed of the gravitational potential energy of m_1

(with the zero point of potential energy being the ground) and the elastic potential energy of the traction gas spring and torsional spring:

$$U = m_1 g(l_4 \sin\theta_0 + l_1 \sin\varphi) + \frac{1}{2}K_1 \Delta S^2 + \frac{1}{2}K_{1r}\Delta\lambda^2, \tag{10}$$

where K_1 is the stiffness coefficient of the traction gas spring and K_{1r} is the stiffness coefficient of the torsional spring.

Therefore, the Lagrange function of the system is

$$
\begin{aligned}
L &= V - U \\
&= \frac{1}{2}m_1 l_1^2 \dot\varphi^2 - m_1 g(l_4 \sin\theta_0 + l_1 \sin\varphi) \\
&\quad - \frac{1}{2}K_1 \Delta S^2 - \frac{1}{2}K_{1r}\Delta\lambda^2.
\end{aligned}
\tag{11}
$$

The dissipative function is

$$
\begin{aligned}
D &= \frac{1}{2}c_1(l'_{BC})^2 + \frac{1}{2}c_{1r}\dot\varphi^2 \\
&= \frac{1}{2}c_1\left(\frac{l_2\dot\varphi\sqrt{l_2^2+l_3^2}\sin(\theta_0+\arctan\frac{l_2}{l_3}+\varphi)}{\sqrt{2l_2^2+l_3^2+2l_2\sqrt{l_2^2+l_3^2}\cos(\theta_0+\arctan\frac{l_2}{l_3}+\varphi)}}\right)^2 \\
&\quad + \frac{1}{2}c_{1r}\dot\varphi^2,
\end{aligned}
\tag{12}
$$

where c_1 is the damping coefficient of the traction gas spring and c_{1r} is the damping coefficient of the torsional spring–damper mechanism.

Then the Lagrange equation of the system can be expressed as

$$\frac{\mathrm{d}}{\mathrm{d}t}\left(\frac{\partial L}{\partial \dot\varphi}\right) - \frac{\partial L}{\partial \varphi} + \frac{\partial D}{\partial \dot\varphi} = 0. \tag{13}$$

By substituting every parameter into the Lagrange equation, after simplification, the motion differential equation for the first-stage buffer system can be determined as follows:

$$
\begin{aligned}
&m_1 l_1^2 \ddot\varphi + K_{1r}(\varphi - \varphi_0) - K_1 l_2 \sin\left(\theta_0 + \arctan\frac{l_2}{l_3} + \varphi\right)\sqrt{l_2^2+l_3^2} \\
&+ m_1 g l_1 \cos\varphi + \frac{K_1 l_2 l_3 \sqrt{l_2^2+l_3^2}\sin(\theta_0+\arctan\frac{l_2}{l_3}+\varphi)}{\sqrt{2l_2^2+l_3^2+2l_2\sqrt{l_2^2+l_3^2}\cos(\theta_0+\arctan\frac{l_2}{l_3}+\varphi)}} \\
&- \frac{c_1 l_2^2 \dot\varphi(l_2^2+l_3^2)(\cos^2(\theta_0+\arctan\frac{l_2}{l_3}+\varphi)-1)}{2l_2^2+l_3^2+2l_2\sqrt{l_2^2+l_3^2}\cos(\theta_0+\arctan\frac{l_2}{l_3}+\varphi)} + c_{1r}\dot\varphi = 0.
\end{aligned}
\tag{14}
$$

Table 1 Design parameters of the first-stage buffer system

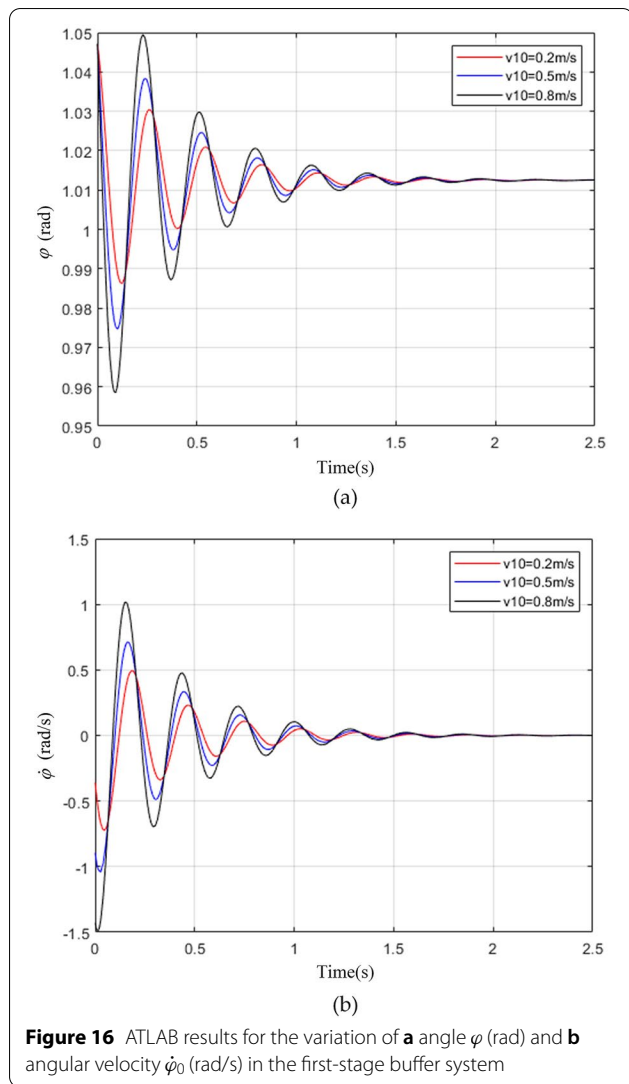| Parameter	Value
m_1 (kg)	12
K_1 (N/m)	1000
K_{1r} (N/(°))	500
c_1 (N·s/m)	25
c_{1r} (N·s/(°))	5
θ_0 (°)	30
φ_0 (°)	60
l_1 (mm)	280
l_2 (mm)	50
l_3 (mm)	120

For application of the first-stage buffer system, we focus on the case of a small motion impact. Because the impact force is small, on account of the momentum theorem, the velocity is relatively low as well. If the initial condition is set inappropriately, the first-stage buffer system will not satisfy the buffer requirement (as is discussed below). Therefore, according to the design parameters given in Table 1, the motion differential equations can be solved with different initial conditions (0.2, 0.5, and 0.8 m/s).

In addition,

$$\dot\varphi_0 = \frac{v_{10}\cos\varphi_0}{l_1}, \tag{15}$$

where v_{10} is the initial condition.

Figure 16 ATLAB results for the variation of **a** angle φ (rad) and **b** angular velocity $\dot{\varphi}_0$ (rad/s) in the first-stage buffer system

The initial condition is equal to the angular velocity of the metacarpal ($\dot{\varphi}_0$). We solved Eq. (14) using MATLAB, and the results are shown in Figure 16.

Because φ is related to the relative height of m_1, the variation of φ reflects the vibration of m_1. The amplitude of m_1 increases with the amplitude of φ. Notice that the angle φ decreases for a period of time when the foot is in contact with the ground. Because the direction of the resultant moment in which the first-stage buffer system and the shank act on the metacarpal is clockwise, the metacarpal rotates clockwise about the supporting point. When the angular velocity becomes zero, the direction of the resultant moment turns anticlockwise. In this case, the metacarpal rotates anticlockwise under the effect of the resultant moment. Finally, the system reaches an equilibrium state after a period of vibration. When the initial velocity increases, the angle and angular velocity also increase. In addition, the vibration frequency becomes higher. Figure 16a and b reflect the buffer effect of the first-stage buffer system, and the vibration trends under different initial velocities are similar.

II. Multistage Buffer System

In this section, the equivalent model of the second-stage buffer system is presented. When the impact is transmitted to the second-stage buffer system, the unidirectional spring of the parallelogram mechanism is compressed. Because of the force transmission character of the parallelogram mechanism, this mechanism proceeds in a translational motion in the sagittal plane, and the force magnitude applied on the parallelogram linkage from the buffer mechanism is equal to the force from the shoulder in the opposite direction. As shown in Figure 17, the second-stage buffer system can be equal to a vibration model with one DOF. m_b is half of the body weight.

When the limb is in the landing process, the wrist joint is locked, and the angle *BAD* is 90°, as shown in Figure 15. Moreover, in the sagittal plane, only the elbow
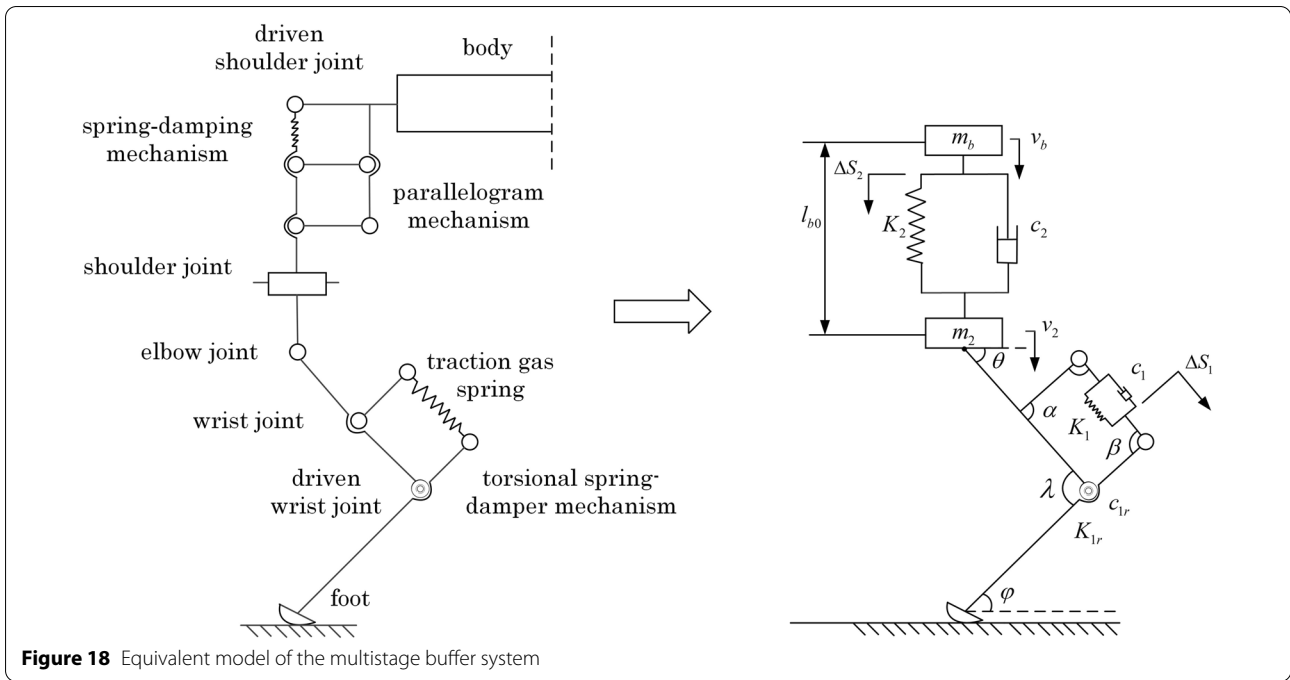

Figure 17 One DOF equivalent vibration model of the second-stage buffer system
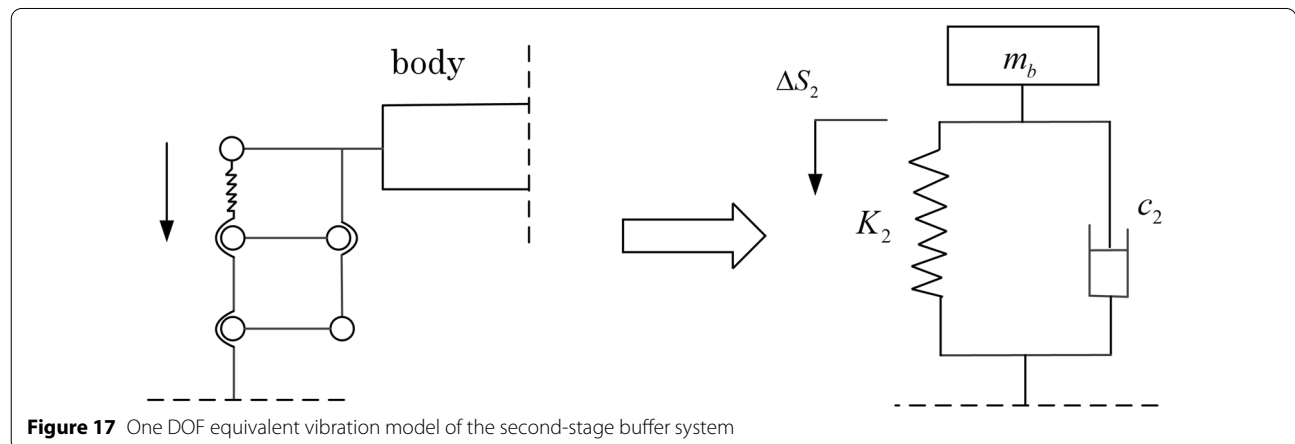
Figure 18 Equivalent model of the multistage buffer system
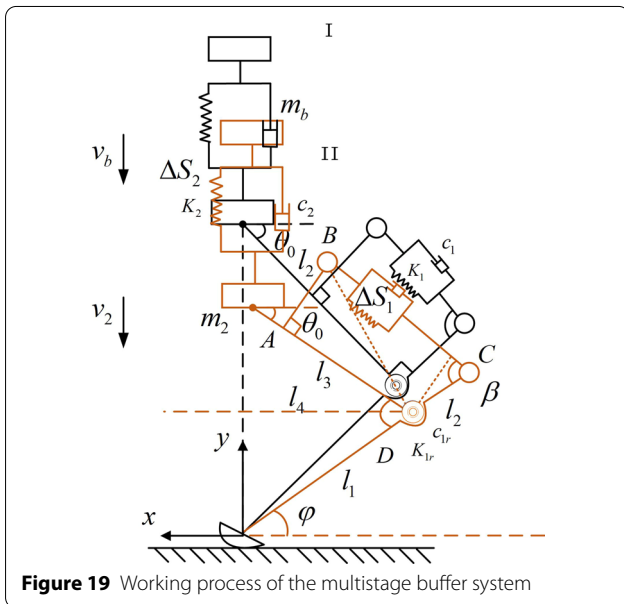

Figure 19 Working process of the multistage buffer system

joint rotates. In this case, the second-stage and first-stage buffer systems form a multistage buffer system together, as shown in Figure 18. In the figure, m_2 is the weight of joints, v_2 is the velocity of m_2, and v_b is the velocity of m_b.

As shown in Figure 19, state I is the initial state of a single limb. In this case, the two buffer systems are both rigid, and the quadrangle *ABCD* is rectangular. The COM of m_2, COM of m_b, and supporting point of the foot are collinear. Moreover, the line connecting these three

points is perpendicular to the horizontal plane. State II is presented as the buffer process for the multistage buffer system. The traction gas spring of the first-stage buffer system is stretched. Meanwhile, the impact is transmitted to the second stage and reaches the stiffness threshold of the spring. Then, the unidirectional spring of the second-stage buffer system is compressed.

Obviously, the entire buffer system has two DOFs. Hence, the generalized coordinates of φ and the generalized position coordinates x_b of m_b, which is relative to m_2 along the vertical direction (coordinate axis y), can be established. The origin was set at the supporting point. The anticlockwise and vertical upward directions were set as positive for φ and x_b.

The analysis of m_2 and the first-stage buffer system is the same as that described in Sect. 2.3.2 I:

$$\Delta S_1 = \Delta S = l_{BC} - l_3$$
$$= \sqrt{2l_2^2 + l_3^2 + 2l_2\sqrt{l_2^2 + l_3^2}\cos(\theta_0 + \arctan\frac{l_2}{l_3} + \varphi)} - l_3,$$
$$(16)$$

$$\Delta\lambda = \varphi - \varphi_0, \tag{17}$$

$$v_{2x} = v_{1x} = l_1\dot\varphi\sin\varphi, \tag{18}$$

$$v_{2y} = v_{1y} = l_1\dot\varphi\cos\varphi, \tag{19}$$

where ΔS_1 is the stretched length of the spring in the first-stage buffer system, as discussed in the previous section.

The velocity v_b can be decomposed into a horizontal component v_{bx} and a vertical component v_{by}. The horizontal displacement of m_b is equal to the displacement of m_2 when the limb changes from I to II. In the second-stage buffer system,

$$\Delta S_2 = x_b - l_{b0}, \tag{20}$$

$$v_{bx} = v_{2x} = l_1\dot{\varphi}\sin\varphi, \tag{21}$$

$$v_{by} = v_{2y} + \dot{x}_b = l_1\dot{\varphi}\cos\varphi + \dot{x}_b, \tag{22}$$

where ΔS_2 is the compressed length of the spring in the spring–damping mechanism and l_{b0} is the initial distance between m_b and m_2.

The kinetic energy of the multistage buffer system is therefore

$$\begin{aligned}
V &= \frac{1}{2}m_2(v_{2x}^2 + v_{2y}^2) + \frac{1}{2}m_b(v_{bx}^2 + v_{by}^2)\\
&= \frac{1}{2}l_1^2\dot{\varphi}^2(m_2 + m_b) + m_b\dot{x}_b l_1\dot{\varphi}\cos\varphi + \frac{1}{2}m_b\dot{x}_b^2.
\end{aligned} \tag{23}$$

The potential energy of the multistage buffer system is composed of the gravitational potential energy of m_b and m_2,

$$U_1 = m_2 g(l_4\sin\theta_0 + l_1\sin\varphi) + m_b g(l_4\sin\theta_0 + l_1\sin\varphi + x_b), \tag{24}$$

and the elastic potential energy of the two independent buffer systems,

$$\begin{aligned}
U_2 &= \frac{1}{2}K_1\Delta S_1^2 + \frac{1}{2}K_{1r}\Delta\lambda^2 + \frac{1}{2}K_2\Delta S_2^2\\
&= \frac{1}{2}K_1\left(\sqrt{2l_2^2 + l_3^2 + 2l_2\sqrt{l_2^2 + l_3^2}\cos(\theta_0 + \arctan\frac{l_2}{l_3} + \varphi)} - l_3\right)^2\\
&\quad + \frac{1}{2}K_{1r}(\varphi - \varphi_0)^2 + \frac{1}{2}K_2(x_b - l_{b0})^2,
\end{aligned} \tag{25}$$

where K_2 is the stiffness coefficient of the spring–damping mechanism.

Therefore, the Lagrange function can be written as

$$\begin{aligned}
L &= V - U = V - U_1 - U_2\\
&= \frac{1}{2}l_1^2\dot{\varphi}^2(m_2 + m_b) + m_b\dot{x}_b l_1\dot{\varphi}\cos\varphi + \frac{1}{2}m_b\dot{x}_b^2\\
&\quad - m_2 g(l_4\sin\theta_0 + l_1\sin\varphi) - m_b g(l_4\sin\theta_0 + l_1\sin\varphi + x_b)\\
&\quad - \frac{1}{2}K_1\left(\sqrt{2l_2^2 + l_3^2 + 2l_2\sqrt{l_2^2 + l_3^2}\cos(\theta_0 + \arctan\frac{l_2}{l_3} + \varphi)} - l_3\right)^2\\
&\quad - \frac{1}{2}K_{1r}(\varphi - \varphi_0)^2 - \frac{1}{2}K_2(x_b - l_{b0})^2.
\end{aligned} \tag{26}$$

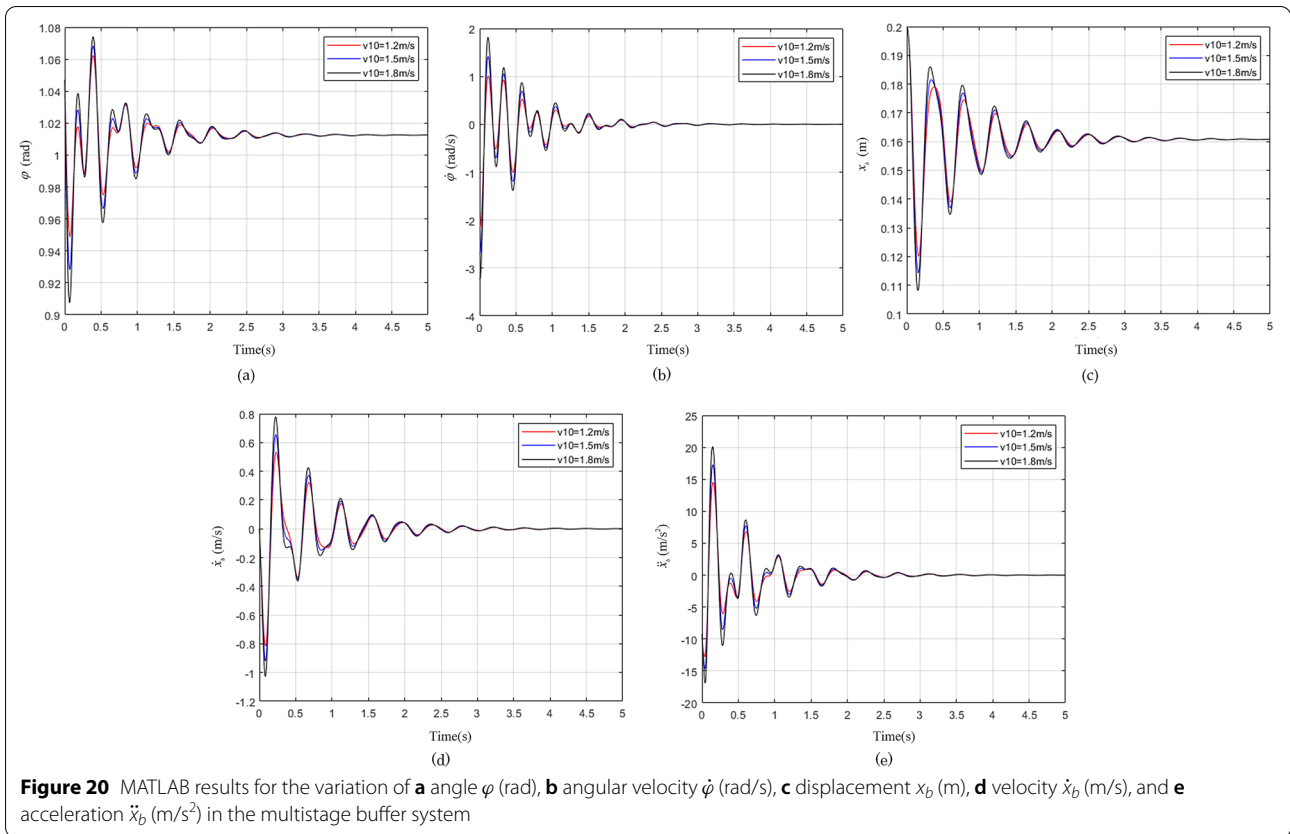**Table 2** Design parameters of the multistage buffer system

Parameter	Value
m_2 (kg)	2
m_b (kg)	10
K_1 (N/m)	1000
K_{1r} (N/(°))	500
c_1 (N · s/m)	25
c_{1r} (N/(°))	5
K_2 (N/m)	2500
c_2 (N · s/m)	50
θ_0 (°)	30
φ_0 (°)	60
l_1 (mm)	280
l_2 (mm)	50
l_3 (mm)	120
l_{b0} (mm)	200

The dissipative function is

$$\begin{aligned}
D &= \frac{1}{2}c_1(l_{bc}')^2 + \frac{1}{2}c_{1r}\dot{\varphi}^2 + \frac{1}{2}c_2 v_b^2\\
&= \frac{1}{2}c_1\left(\frac{l_2\dot{\varphi}\sqrt{l_2^2 + l_3^2}\sin(\theta_0 + \arctan\frac{l_2}{l_3} + \varphi)}{\sqrt{2l_2^2 + l_3^2 + 2l_2\sqrt{l_2^2 + l_3^2}\cos(\theta_0 + \arctan\frac{l_2}{l_3} + \varphi)}}\right)^2\\
&\quad + \frac{1}{2}c_{1r}\dot{\varphi}^2 + \frac{1}{2}c_2\dot{x}_b^2,
\end{aligned} \tag{27}$$

where c_2 is the damping coefficient of the spring–damping mechanism.

Then, the Lagrange equations of the system can be expressed as

Figure 20 MATLAB results for the variation of **a** angle φ (rad), **b** angular velocity $\dot{\varphi}$ (rad/s), **c** displacement x_b (m), **d** velocity $\dot{x}_b$ (m/s), and **e** acceleration $\ddot{x}_b$ (m/s^2) in the multistage buffer system

$$\frac{\mathrm{d}}{\mathrm{d}t}\left(\frac{\partial L}{\partial \dot{\varphi}}\right) - \frac{\partial L}{\partial \varphi} + \frac{\partial D}{\partial \dot{\varphi}} = 0, \tag{28}$$

$$\frac{\mathrm{d}}{\mathrm{d}t}\left(\frac{\partial L}{\partial \dot{x}_b}\right) - \frac{\partial L}{\partial x_b} + \frac{\partial D}{\partial \dot{x}_b} = 0. \tag{29}$$

By substituting every parameter into the Lagrange equations, after simplification, the motion differential equations of the multistage buffer system can be determined as Eq. (30).

For the application of the multistage buffer system, we focus on the case of a relatively large motion impact. As discussed above, a larger impact force means a higher velocity. Therefore, the initial velocity of the multistage buffer system can be higher than that of the first-stage buffer system. According to the design parameters given in Table 2, the motion differential equations with different initial conditions (1.2, 1.5, and 1.8 m/s) can be solved. The results are presented in Figure 20.

Figures 20a and b indicate that an abnormal vibration of the first buffer system appears during 0.6–0.8 s. With the increase of v_{10}, the amplitudes of φ and $\dot{\varphi}$ grow bigger. The vibration trend of φ first decreases, as does that of $\dot{\varphi}$. However, the variation of x_b in the second-stage buffer system remains normal. The trend of vibration amplitudes of x_b is decrescent. After the system vibrates for a period of time, x_b is finally stabilized at 160 mm. However, the trends of vibration amplitudes of velocity and acceleration are abnormal, unlike the displacement, as shown in Figure 20c–e.

To understand the buffer effect of using the first-stage buffer system or multistage buffer system individually under the cases of small impact conditions and large impact conditions, cases of 0.8 and 1.8 m/s were compared. The results are shown in Figure 21.

if the motion impact is small, the impact buffer effect of the multistage buffer system, in which the second-stage buffer system is not locked, is similar to that of the first-stage buffer system or even worse.

According to Figure 21b, the amplitudes of φ in the

$$\begin{cases} (m_2+m_b)l_1^2\ddot{\varphi}+m_bl_1\ddot{x}_b\cos\varphi+K_{1r}(\varphi-\varphi_0)+(m_2+m_b)gl_1\cos\varphi+c_{1r}\dot{\varphi}-K_1l_2\sqrt{l_2^2+l_3^2}\sin(\theta_0+\arctan\frac{l_2}{l_3}+\varphi) \\[4mm] +\dfrac{K_1l_2l_3\sqrt{l_2^2+l_3^2}\sin(\theta_0+\arctan\frac{l_2}{l_3}+\varphi)}{\sqrt{2l_2^2+l_3^2+2l_2\sqrt{l_2^2+l_3^2}\cos(\theta_0+\arctan\frac{l_2}{l_3}+\varphi)}}-\dfrac{c_1l_2^2\dot{\varphi}(\cos^2(\varphi+\theta_0+\arctan\frac{l_2}{l_3})-1)(l_2^2+l_3^2)}{2l_2^2+l_3^2+2l_2\sqrt{l_2^2+l_3^2}\cos(\theta_0+\arctan\frac{l_2}{l_3}+\varphi)}=0, \quad (30) \\[4mm] \qquad\qquad m_bl_1\ddot{\varphi}\cos\varphi+m_b\ddot{x}_b-m_bl_1\dot{\varphi}^2\sin\varphi-\frac{1}{2}(K_2(2l_{b0}-2x_b))+m_bg+c_2\dot{x}_b=0. \end{cases}$$

As shown in Figure 21a, the amplitudes of φ in the multistage buffer system are larger than those in the first-stage buffer system at some moments. This indicates that,

multistage buffer system are smaller than those in the first-stage buffer system. This result suggests that, when the initial velocity of the limb increases unceasingly, the amplitudes of φ in the first-stage buffer system will converge to zero. In other words, the valley value of φ in the first-stage buffer system will become negative. In this case, the first-stage buffer system cannot satisfy the requirement of the buffer, but the multistage buffer system can still work properly. Therefore, the impact buffer effect of the multistage system is better than that of the first-stage system.

3 Results and Discussion
In this section, the detailed mechanical structure design of a robot leg with a configuration that contains the multistage buffer system is completed. Based on this robot leg, we designed a quadruped robot and performed simulation experiments to verify the effectiveness of the multistage buffer system.

3.1 Virtual Prototype Design
As shown in Figure 22, a three-dimensional leg prototype based on modeling software (SolidWorks) was designed. This leg configuration includes three joints, as shown in the schematic diagrams of the mechanism discussed in Section 2.3.1. Some accessories, such as bolts and encoders, are not displayed. The main driving elements were the three motors. Figure 23a shows the mechanical structure of the second-stage buffer system with a parallelogram mechanism. The spring is fixed on a position-limitation mechanism and can only be compressed. The parallelogram mechanism with the traction gas spring of the first-stage buffer system is shown in Figure 23b, and the torsional spring–damper mechanism is mounted on the driven wrist joint. The size design of the leg prototype was based on the parameters presented in the previous sections.
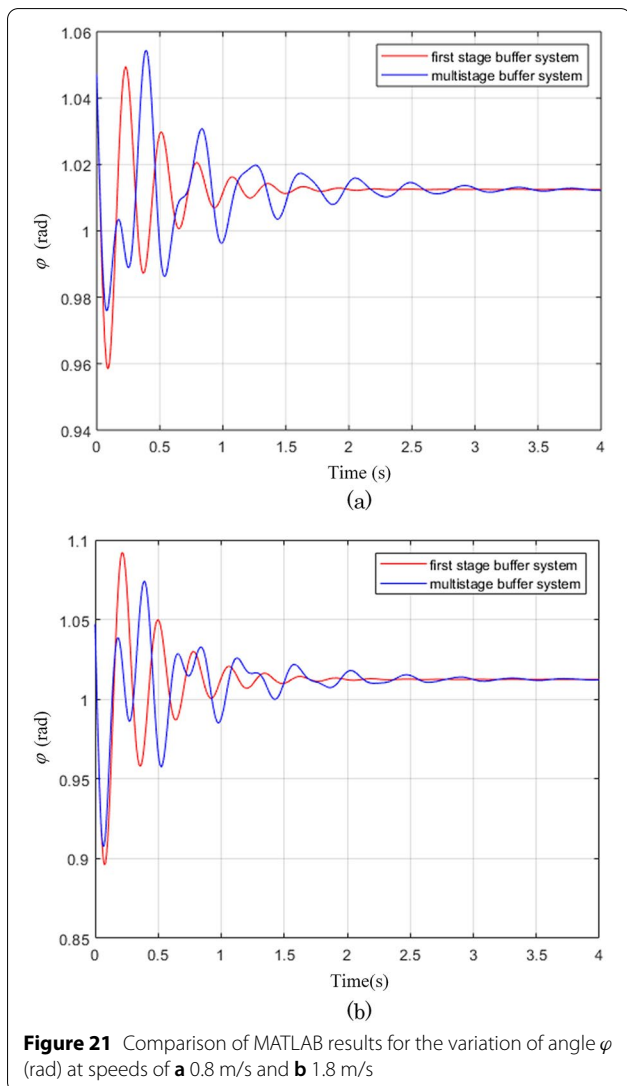

Figure 21 Comparison of MATLAB results for the variation of angle φ (rad) at speeds of **a** 0.8 m/s and **b** 1.8 m/s
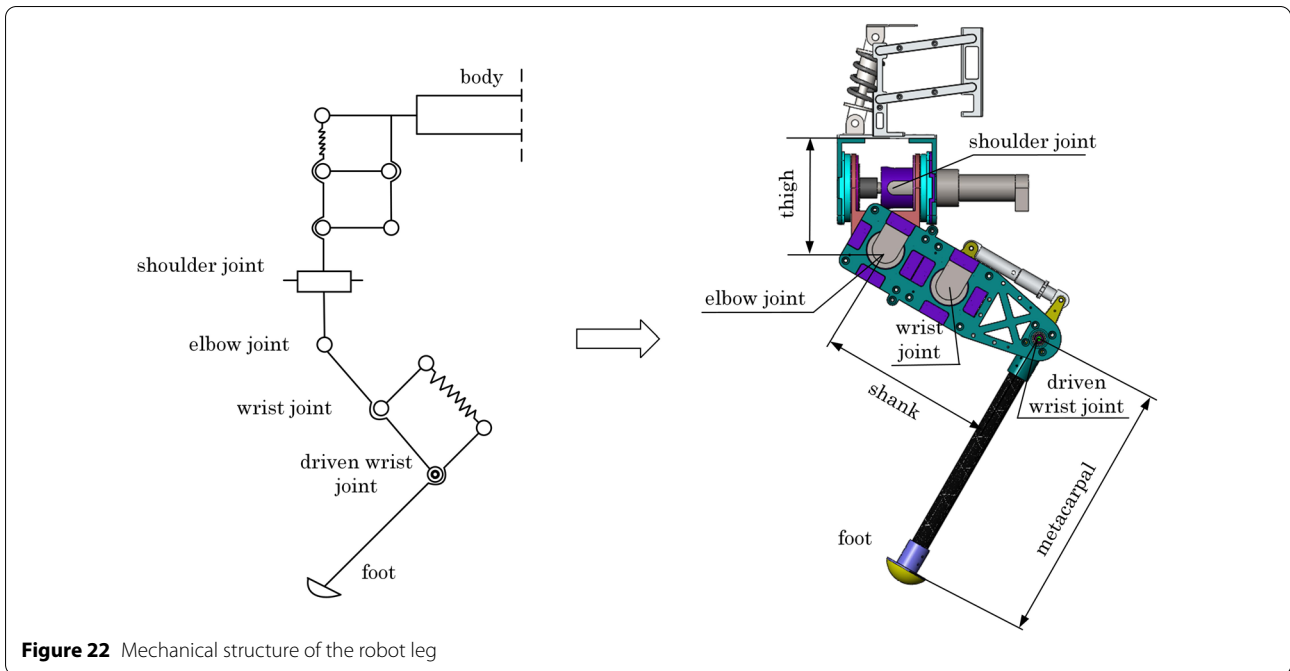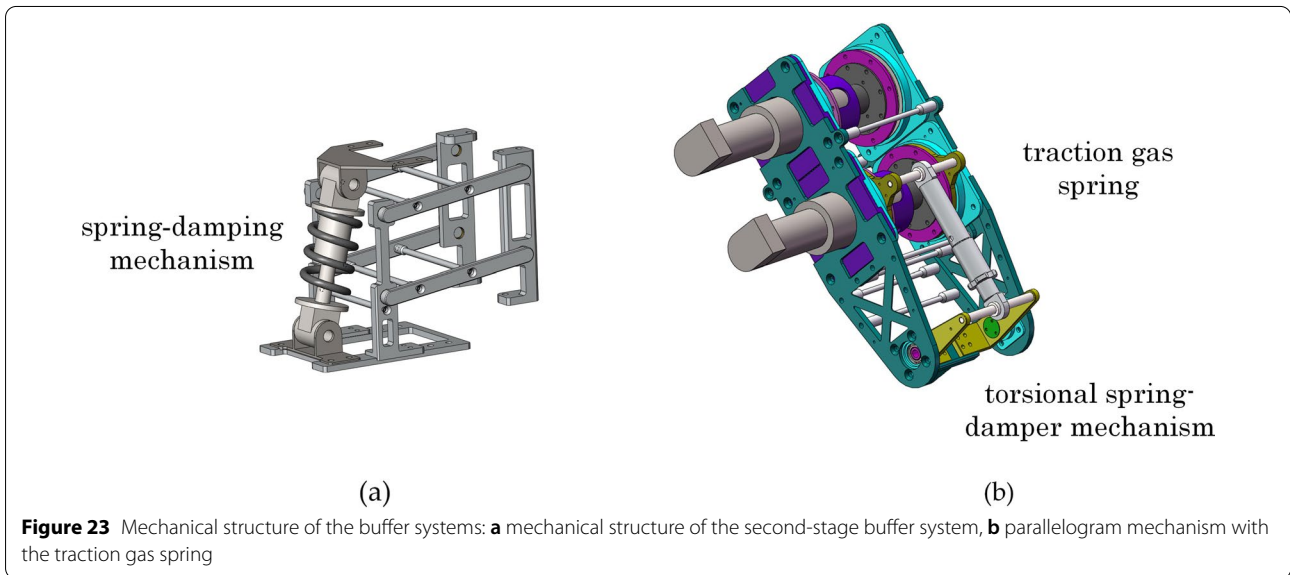
Figure 22 Mechanical structure of the robot leg

Figure 23 Mechanical structure of the buffer systems: **a** mechanical structure of the second-stage buffer system, **b** parallelogram mechanism with the traction gas spring

Based on this leg structure design, a quadruped robot was developed, and the virtual prototype is shown in Figure 24. Both the leg prototype design and quadruped robot prototype design are in line with the parameters listed in Tables 1 and 2. The basic parameters of the quadruped robot elements are listed in Table 3. In addition to the body mechanical frame, the mass of the body includes accessories such as the control module, various sensors, and batteries, which are not displayed. Moreover, the material of the metacarpal is carbon fiber, and the

mass of the metacarpal can be ignored compared with that of other parts.

3.2 Simulation Experiments

The buffer effects of different systems in the same case are discussed next. First, the format of the virtual prototype was transferred from the SLDASM to x_t in Solid-Works. Then, we imported the virtual prototype of the quadruped robot into ADAMS and set up the simulation environment, including the settings of the contact force
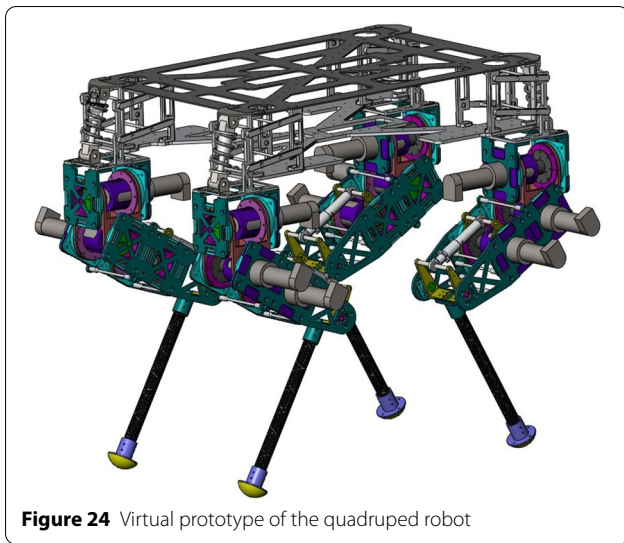
Zheng *et al. Chinese Journal of Mechanical Engineering*   (2022) 35:32

Page 18 of 21

Figure 24 Virtual prototype of the quadruped robot

Table 3 Basic parameters of the quadruped robot elements

Component	Size (mm or mm×mm×mm)	Mass (kg)
Body	600×400×100	20
Thigh	130	0.2
Shank	200	1.8
Metacarpal	280	0.05

and friction force, as shown in Figure 25. The robot body was parallel to the ground in the initial state. Moreover, in the sagittal plane, the angles of the shank and shoulder joint rotation axis to the metacarpal were 30° and 90°, respectively, at the beginning. The collision between the foot end and ground was considered to be elastic.

To realize the robot trotting gait at 0.6 m/s, based on the composite cycloid trajectory planning method of the foot end [30] and the inverse kinematics of a single leg [31], each driving angle of the elbow joint and wrist joint must be determined. Then, according to the inner-wrist type of limb and the phase difference of the trot, we applied a spline to add the driving function for each driving joint.

Before we collect useful data from the simulation experiments, we need to confirm the metric used to validate our solution. In addition to the classic pendulum model [32], some scholars have conducted further research on the spring–mass system for animal running and jumping. A mathematical analysis has been given, and the time-varying variation curves of the COM displacement and contact force have been presented to evaluate the motion performance [33]. Therefore, the motion performance of the robot can be denoted by the smoothness of the COM, which is derived from the derivation of the body COM acceleration and the contact force applied to the leg.

Three experimental cases—walking with the first-stage buffer system, walking the multistage buffer system, and walking without the buffer system—were studied in ADAMS. The acceleration variation of the robot body along the vertical direction indicates the force condition applied to the robot body. Figure 25 shows the acceleration variation of the robot body COM for the three cases with a trotting gait.

Obviously, the COM acceleration variation fluctuates acutely when the robot is walking without a buffer system. In this case, most of the external force is transmitted to the body through the rigid parts, damaging the mechanical structure. Figure 26a proves the correctness
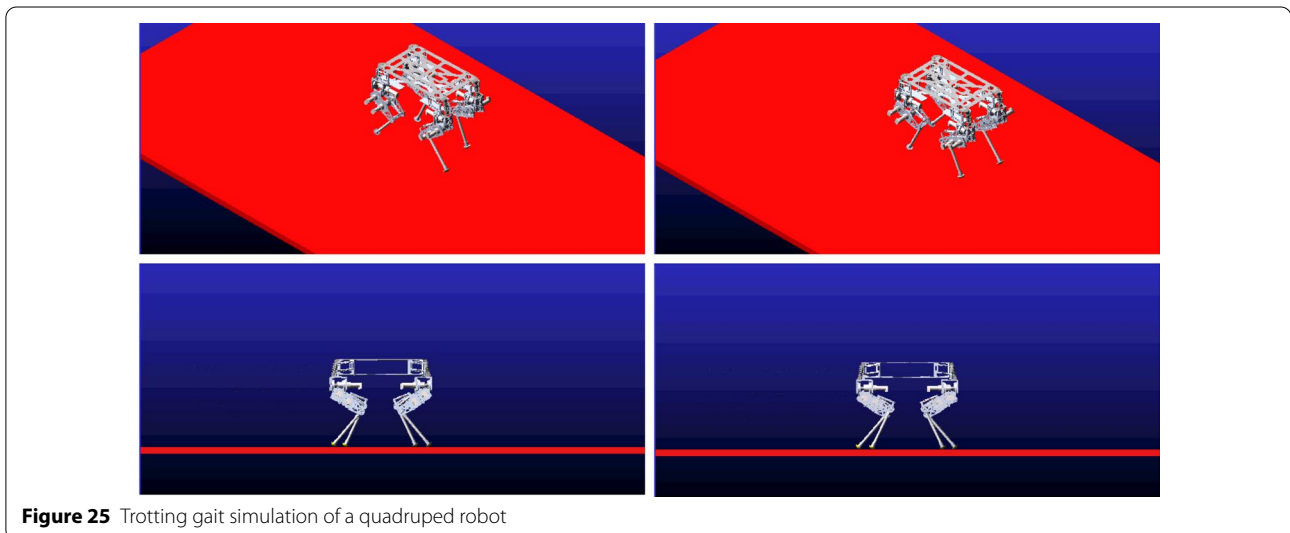

Figure 25 Trotting gait simulation of a quadruped robot

Zheng *et al. Chinese Journal of Mechanical Engineering* (2022) 35:32
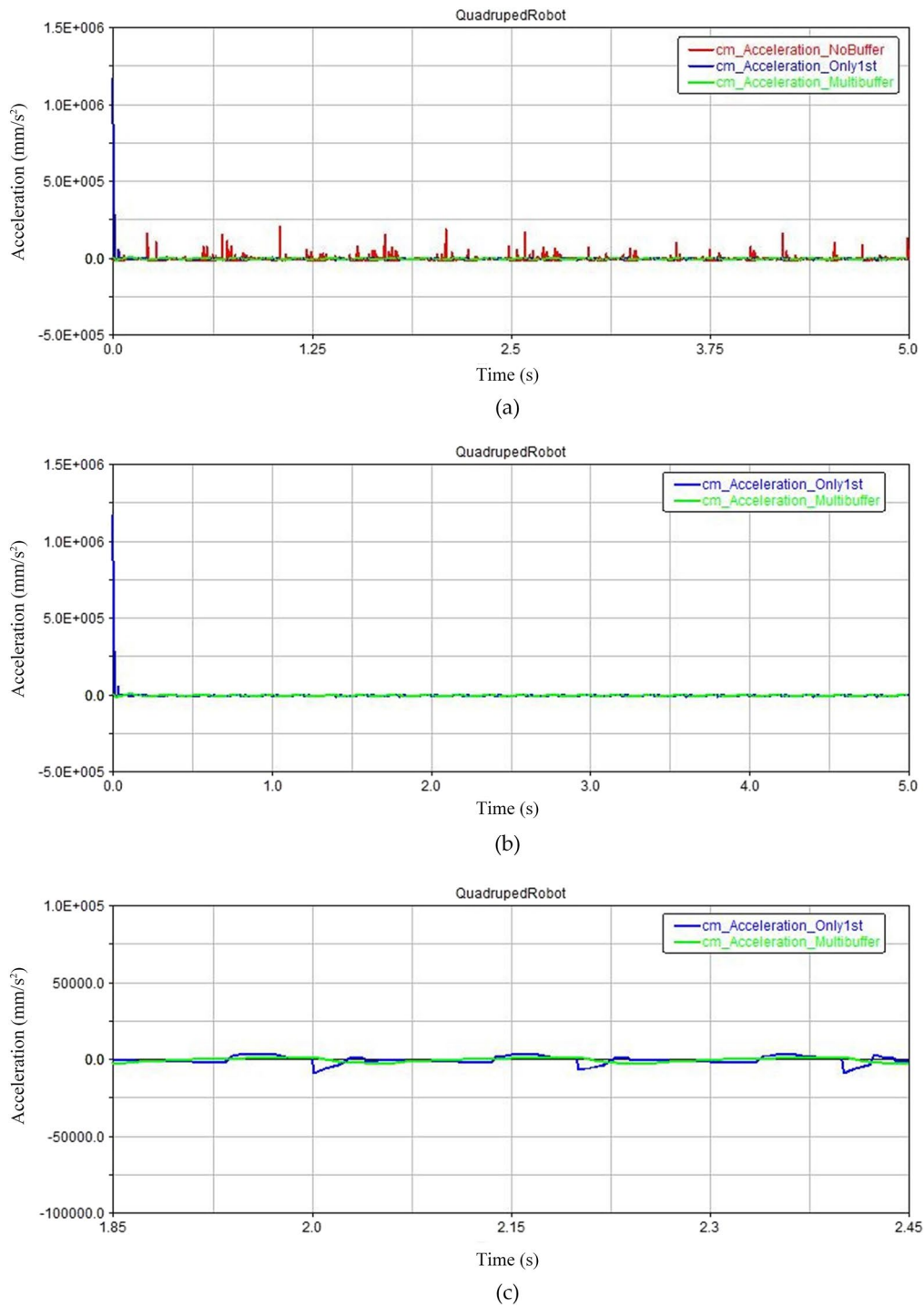
Page 19 of 21

Figure 26 ADAMS simulation results: **a** acceleration variation of the robot COM in three cases, **b** acceleration variation comparison between the two latter cases, **c** walking process curves between 1.85 and 2.45 s for the two latter cases
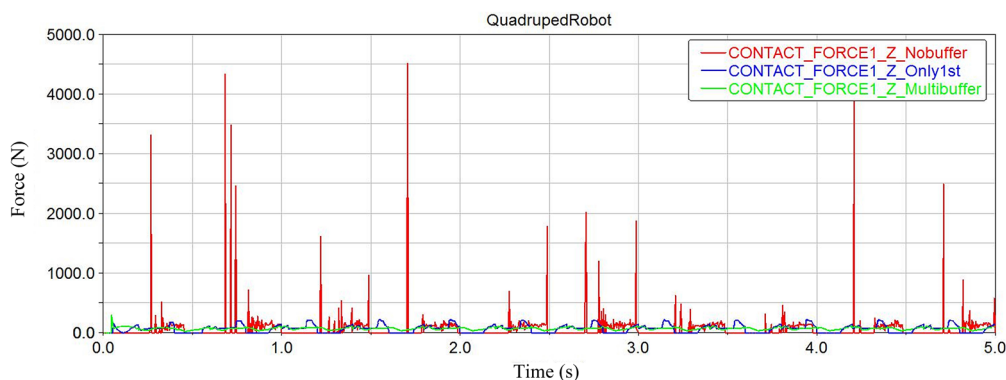
Figure 27 Contact force variation comparison of the three cases

of this inference; the COM acceleration variation in the left two cases is less than in the first case in which walking is done without a buffer system. For further discussion, the curves of walking with the first-stage buffer system and walking with the multistage buffer system are shown in Figure 26b. Notice that the COM acceleration variation of the former walking case exhibits a sudden increase at the beginning. In Figure 26c, we cut the walking process between 1.85 and 2.45 s to compare these two curves clearly. The result indicates that the COM acceleration variation in the case of walking with a multistage buffer system is smoother and that the mean value of acceleration is smaller.

Moreover, the contact force applied to the right forelimb along the *z* axis in these three cases was measured, as shown in Figure 27. The result is similar to the acceleration variation: The contact force in the case of walking without the buffer system exhibits a great variation in amplitude and the multistage buffer system smooths the variation in the contact force compared with that in the other cases.

The analysis of COM acceleration and contact force indicates that, when the robot walks with the same gait and velocity on a flat surface, the multistage buffer system produces a smoother walking process, and this kind of buffer system has a better buffering effect on vibration compared with the buffer with only a single stage.

4 Conclusions

Owing to its great similarity to a walking animal, the legged robot has become a popular subject for seeking better flexibility and stability while passing through wild terrain. Specifically, some field operations without humans, such as field surveys, material transportation, and emergency rescue, require robots to exhibit outstanding motion performance. Motion impact buffering

is a crucial aspect that affects the motion performance. The lack of motion impact buffering may cause unnecessary energy loss or damage to the mechanical structure of the robot.

To solve the problems mentioned above, the following aspects were addressed:

(1) We explored the multiple buffer parts in ruminant limbs through the animal anatomy of the musculoskeletal system.
(2) Based on the bionics principle, bionic mapping models of buffer systems were presented.
(3) After analyzing the biology and bionics, we presented the first-stage buffer system mechanism design. The second-stage buffer system, which is inspired by the shoulder musculoskeletal system of a ruminant, is an innovative buffer system mechanism design. The mechanism design of the multistage buffer system was then completed.
(4) The buffer effects of a first-stage buffer system and multistage buffer system were compared theoretically by analysis of their mechanisms.
(5) In addition, after designing the detailed mechanical structure of the robot limb and virtual prototype, we compared the buffer effects of three cases by simulation experiments. The results indicate that the impact buffer effect of the multistage buffer system is ideal and enables a smooth transit of the COM both in theory and in the simulations.

In conclusion, the novel limb design with a multistage buffer system is a better choice for legged robots and presents a design template for limb buffer systems in applications in the fields mentioned above.

Zheng *et al. Chinese Journal of Mechanical Engineering*   (2022) 35:32

Page 21 of 21

Authors' Information
Yi Zheng, born in 1991, is currently a PhD candidate at *Space Robot Laboratory, School of Mechanical Engineering and Automation, Beihang University, China*. He received his bachelor degree and master degree from *Hefei University of Technology, China*, in 2013 and 2016 respectively. His research interests include biomimetic robots and mechanical design.

Kun Xu, born in 1981, is currently an associate professor at *Space Robot Laboratory, School of Mechanical Engineering and Automation, Beihang University, China*. He received the B.Eng. degree in mechanical design and manufacture, the M.Eng. degree in mechanical engineering, and the Ph.D. degree in mechanical design and theory from *Beihang University, Beijing, China*, in 2005, 2008, 2012, respectively. His research interests include robotics, mechanism, biomimetic design, and manufacture.

Yaobin Tian, born in 1986, is currently a lecturer at *Space Robot Laboratory, School of Mechanical Engineering and Automation, Beihang University, China*. His research interests include robotics, modular robot and mechanism.

Huichao Deng, born in 1985, is currently a lecturer at *Space Robot Laboratory, School of Mechanical Engineering and Automation, Beihang University, China*. Her research interests include flapping wing flying robot, mechatronics and mechanism.

Xilun Ding, born in 1967, is currently a professor at *Beihang University, China*. He received his PhD degree from *Harbin Institute of Technology, Harbin, China*. His research interests include the dynamics of compliant mechanical systems and robots, nonholonomic control of pace robots, dynamics and control of aerial robots, and biomimetic robots. Tel: +86-010-82339005.

References
[1] R McN Alexander. Three uses for springs in legged locomotion. *The International Journal of Robotics Research*, 1990, 9(2): 53–61.
[2] S Tripathy, S Gaur. Rough terrain quadruped robot-BigDog. *Materials Today: Proceedings*, 2021.
[3] R X Liu. *Structural design and simulation optimization of quadruped robot*. Beijing: North China University of Technology, 2017. (in Chinese)
[4] J H Han. *Control strategy based on flying trot gait for running quadruped robot*. Harbin: Harbin Institute of Technology, 2019. (in Chinese)
[5] J Y Liu. From big dog to spot mini: Evolution of boston powered quadruped robot. *Robot Industry*, 2018, 2: 109–116. (in Chinese)
[6] Y N Zhang, M Q An. Structure and software architecture design of an extremely low-cost quadruped robot for education. *Journal of Physics: Conference Series*, 2021, 1931(1): 012007.
[7] L H Ding. Key Technology analysis of BigDog quadruped robot. *Journal of Mechanical Engineering*, 2015, 51(7): 1–23. (in Chinese)
[8] C Gehring, S Coros, M Hutter, et al. Practice makes perfect: An optimization-based approach to controlling agile motions for a quadruped robot. *IEEE Robotics & Automation Magazine*, 2016, 23(1): 34–43.
[9] M Wermelinger, P Fankhauser, R Diethelm, et al. Navigation planning for legged robots in challenging terrain. *IEEE/RSJ International Conference on Intelligent Robots and Systems (IROS)*, Daejeon, 2016: 1184–1189.
[10] X R Meng, S Wang, Z Q Cao, et al. A review of quadruped robots and environment perception. 35*th Chinese Control Conference (CCC)*, Chengdu, 2016: 6350–6356.
[11] T Chen, X B Sun, Z Xu, et al. A trot and flying trot control method for quadruped robot based on optimal foot force distribution. *Journal of Bionic Engineering*, 2019, 16(4): 621–632.
[12] L Wagner, P Fankhauser, M Bloesch, et al. Foot contact estimation for legged robots in rough terrain. *Advances in Cooperative Robotics*, 2017: 395–403.
[13] D J Hyun, J Lee, S I Park, et al. Implementation of trot-to-gallop transition and subsequent gallop on the MIT Cheetah I. *The International Journal of Robotics Research*, 2016, 35(13): 1627–1650.
[14] G Bledt, P M Wensing, S Kim. Policy-regularized model predictive control to stabilize diverse quadrupedal gaits for the mit cheetah. *IEEE/RSJ International Conference on Intelligent Robots and Systems (IROS)*, Vancouver, 2017: 4102–4109.
[15] S W Heim, M Ajallooeian, P Eckert, et al. On designing an active tail for legged robots: Simplifying control via decoupling of control objectives. *Industrial Robot: An International Journal*, 2016.
[16] G S Kumar, S Aravind, R Subramanian, et al. Literature Survey on Four-Legged Robots. *Trends in Mechanical and Biomedical Design*, 2021: 691–702.
[17] P Eckert. *Towards agility: Definition, benchmark and design considerations for small, quadrupedal robots*. Lausanne: EPFL, 2018.
[18] M Zieliński, D Belter. Mechanical design and control of compliant leg for a quadruped robot. *Advances in Intelligent Systems and Computing*, 2018, 743: 500–509.
[19] P Eckert, A E M Schmerbauch, T Horvat, et al. Towards rich motion skills with the lightweight quadruped robot serval–a design, control and experimental study. *International Conference on Simulation of Adaptive Behavior*, Frankfurt, 2018: 41–55.
[20] D H Chadwick. *A beast the color of winter: The mountain goat observed*. Lincoln: University of Nebraska Press, 2002.
[21] B L Smith. *Life on the rocks: A portrait of the mountain goat*. Washington DC: Rowman & Littlefield, 2020.
[22] M Doube, A A Felder, M Y Chua, et al. Limb bone scaling in hopping macropods and quadrupedal artiodactyls. *Royal Society open science*, 2018, 5(10): 180152.
[23] Q Zhang. *Study on anti-slip and buffer characteristics of goat foot and design of bionic foot*. Changchun: Jilin University, 2019. (in Chinese)
[24] H E Koenig, R Korbel, H G Liebich, et al. *Avian anatomy: Textbook and colour atlas*. Sheffield: 5m Books Ltd, 2016.
[25] Q Zhang, K Xu, X L Ding. Investigation of feet functions of large ruminants with a decoupled model of equivalent mechanism. *Biology Open*, 2017, 6(4): 407–414.
[26] Q Zhang, X L Ding, K Xu. Terrain adaptability mechanism of large ruminants' feet on the kinematics view. *Applied Bionics and Biomechanics*, 2015, 2015: 1–9.
[27] R R Ashdown, S H Done, S W Barnett. *Color atlas of veterinary anatomy, volume 1, the ruminants e-book*. Amsterdam: Elsevier Health Sciences, 2010.
[28] K Xu, X L Ding. Typical gait analysis of a six-legged robot in the context of metamorphic mechanism theory. *Chinese Journal of Mechanical Engineering*, 2013, 26(4): 771–783.
[29] X L Ding, Y Zheng, K Xu. Wheel-legged hexapod robots: A multifunctional mobile manipulating platform. *Chinese Journal of Mechanical Engineering*, 2017, 30(1): 3–6.
[30] Y Sakakibara, K Kan, Y Hosoda, et al. Foot trajectory for a quadruped walking machine. *IEEE International Workshop on Intelligent Robots and Systems, Towards a New Frontier of Applications*, Ibaraki, 1990: 315–322.
[31] K M Lynch, F C Park. *Modern robotics: Mechanics, planning, and control*. Cambridge: Cambridge University Press, 2017.
[32] G A Cavagna, N C Heglund, C R Taylor. Mechanical work in terrestrial locomotion: two basic mechanisms for mini-mizing energy expenditure. *American Journal of Physiology-Regulatory, Integrative and Comparative Physiology*, 1977, 233(5): R243-R261.
[33] R Blickhan. The spring-mass model for running and hopping. *Journal of Biomechanics*, 1989, 22(11-12): 1217-1227.